1.23 Deep Earth Structure: The Earth's Cores

A Souriau and M Calvet, CNRS and Université Paul Sabatier, Toulouse, France

This chapter is a revision of the previous edition chapter by A Souriau, Volume 1, pp. 655–693, © 2007, Elsevier B.V.

1.23.1 Introduction

The Earth's core represents 16% of the volume of the Earth and more than 30% of its mass. It is composed of an iron alloy that incorporates light elements and nickel. At the center of this wide ocean of iron, the solid inner core, of about the size of the moon, represents only 4.3% of the volume of the core and $<1\%$ of the volume of the Earth. It results from the freezing of the liquid core during the cooling of the Earth, with a strong depletion in light elements. The core plays a very important role in Earth physics and chemistry. However, despite its impact on many physical processes such as magnetic field and the Earth's rotation, which have been investigated for centuries, the core has been detected very late, in 1906, when the seismological observation of the deep Earth became possible. Since then, important advances have been made, combining observations, laboratory experiments, and theoretical modeling. But the core remains enigmatic. If some of the core

properties are now firmly established, many others are still controversial. This chapter will attempt to give a survey of the present state of the art, trying to give a degree of confidence to the various results.

Before going through the details of the core structure, it is useful to recall some basic information concerning the core, which in addition shows its importance in the planet Earth system. The core is governed by complex systems of relations implying thermodynamics, hydrodynamics, geomagnetism, and geochemistry. Advances and results concerning these different disciplines may be found in other chapters of this treatise, in particular **Chapters 2.06**, **3.10**, **8.02**, **8.04–8.09**, **8.12**, **8.13**, **9.03**, and **9.08**.

The core forms very early in the history of our planet, as revealed by the analyses of lead and uranium mantle isotopes and other radionuclide chronometers and by the presence of a magnetic field in the oldest rocks of the Earth, 3.5 Ga old. It is generally accepted that the inner core formed by crystallization of the liquid core. Some thermodynamic arguments favor a rather young inner core, about 1 Ga old, but this is still open to discussion.

Convection in the liquid core is at the origin of the main part of the magnetic field. From this point of view, the core is essential to the life, as it protects the Earth from the solar wind. Numerical simulations of the Earth geodynamo show that the inner core has probably a stabilizing role for the magnetic field, as it prevents frequent geomagnetic reversals.

The boundary of the core with the silicate mantle, the core–mantle boundary (CMB), is a place of thermal, dynamic, and probably chemical exchanges. In particular, the exchange of angular momentum influences the Earth's rotation. At the inner core boundary (ICB), the freezing of the liquid iron alloy occurs with a depletion of the light elements that are present in the liquid core. The ICB is thus also an important place for chemical and energy exchanges. Heat sources linked to inner core growth, including latent heat and gravitational energy, are essential for powering the geodynamo and are important factors in the thermal history of the Earth.

In what follows, we will only consider the aspects relevant to the structure of the core, giving a particular importance to seismology, which has provided most of the results obtained today about its internal properties. After a brief historical review, we will present the most usual tools used in core seismology. The radial structure of the core will then be investigated, paying particular attention to the core boundaries. Then, a large section will concern the inner core, for which different properties will be considered: its rigidity; its anisotropy for both velocity and attenuation; its hemispherical dichotomy, which also concerns both velocity and attenuation; and its possible differential rotation or oscillation with respect to the mantle. We will end this chapter with the still open questions and future challenges.

1.23.2 The Discovery of the Core

Scientific arguments coming from astronomical and geological observations and theoretical developments concerning heat propagation, thermodynamics, geodesy, and mechanics led to the proposal that the Earth is stratified, with a silicate mantle and an iron core. But the specification of core properties is mostly derived from seismological observations. Combined with mineral physics, they have allowed us to obtain the present picture of the Earth, made of a silicate mantle, an iron liquid core, and a solid iron inner core, with a radius of 3480 km (0.55 ×Earth radius) for the CMB and a radius of 1220 km (0.19 ×Earth radius) for the ICB.

1.23.2.1 Indirect Evidences for the Existence of a Core and Historical Controversies

The fascination for the Earth's interior is present in the literature since the antiquities (see historical aspects in Brush, 1980; Bolt, 1982; Deparis and Legros, 2002). During the nineteenth century, it is generally accepted that the Earth has been fluid at its origin. This idea resulted mostly from the observation of the Earth flattening, an equilibrium figure supposed to be acquired during fluid stage, and from the identification of plutonic rocks. The question was raised of whether the Earth is still fluid in its interior, or solid as a result of its complete cooling, or partly solid. The geothermal gradient measured at the surface (about 30 °C km^{-1}) predicts a melting of the Earth silicates at about 80–100 km depth, an idea reinforced by the fluid lavas rejected by volcanoes. An argument against this model is given by Ampère (1775–1836), who noted that such a structure would not be able to support the high stresses induced by the lunar tides on the thin solid envelope. On the other hand, Poisson (1781–1840) noted that the melting temperature of rocks increases with pressure, opening the possibility of a completely solid Earth.

Two discoveries have allowed us to reconcile a solid Earth model with the high geothermal gradient: first, the idea that the internal heat is eliminated not only by conduction but also (and mostly) by convection and, second, the discovery of radioactivity as a source of internal heat, in addition to the initial heat. These two discoveries explain the impossibility of extrapolating the upper crust geothermal gradient downward. On the other hand, the comparison of the precession and nutations of the Earth observed from astronomy with those computed for different structures led Hopkins (1793–1866) to propose a solid envelope of at least 1000 km thickness, the fluid center being thus much too deep for being the feeding region of the volcanoes. More refined computations by Kelvin (1824–1907) gave a 2000–2500 km thickness for the solid envelope.

The mean density of the Earth, 5.52×10^3 kg m^{-3}, is much higher than that of the rocks (about 2.6×10^3 kg m^{-3} for granite), even at the temperature and pressure conditions present at 2500 km depth. Its moment of inertia, $I = 0.33\ Ma^2$, where M is the mass of the Earth and a its radius, is smaller than that of a homogeneous sphere ($I = 0.40\ Ma^2$), implying high densities at depth, thus a chemical differentiation. Geochemical arguments, in particular cosmic abundances and the existence of both silicate and iron meteorites, led to propose an iron core. Stony-iron meteorites such as pallasites may represent the CMB. At the end of the nineteenth century, a model with a silicate mantle above an iron core was widely accepted (e.g., Wiechert, 1896).

The effective detection of the core is, however, attached to seismology. In 1889, the first recording of a remote earthquake opened the possibility of sampling deep Earth structure with teleseismic data. This discovery stimulated the deployment of worldwide observatories and the international organization of seismology (see **Chapter 1.01**).

1.23.2.2 The Seismological Detection of the Liquid Core and Inner Core

Most of the teleseismic records exhibit two clear arrivals, a primary, compressional phase (P), and a secondary, shear phase (S). Oldham (1906) noted that the propagation time of the S-wave as a function of distance was delayed by about 10 min for angular distances larger than 130°. He ascribed this delay to the propagation through a core in which the velocity is smaller than in the mantle, due to a change in physical properties. Although the observed late phase was not S, but SS (an S phase reflected once beneath the surface), this observation led to consider that Oldham is the discoverer of the core. Gutenberg (1913) determined the depth of the CMB at 2900 km, a value that has not significantly changed later. The fluidity of the core was confirmed by Jeffreys (1926) thanks to the evaluation of the mean Earth rigidity deduced from Earth tides, which is lower than the mantle rigidity deduced from seismic wave propagation. The nature of this core, mostly made of fluid iron, was established by Birch (1952, 1964), a pioneer in high-pressure physics, who demonstrated that a silicate at pressure and temperature similar to core conditions could not reach the inferred mass density of about 10^4 kg m^{-3}.

The discovery of the inner core is due to Lehmann (1936), who detected a seismic phase arrival at a distance where no P-phase is supposed to arrive, in a distance range (about 110–140°) called the shadow zone of the core (**Figure 1(a)**). She

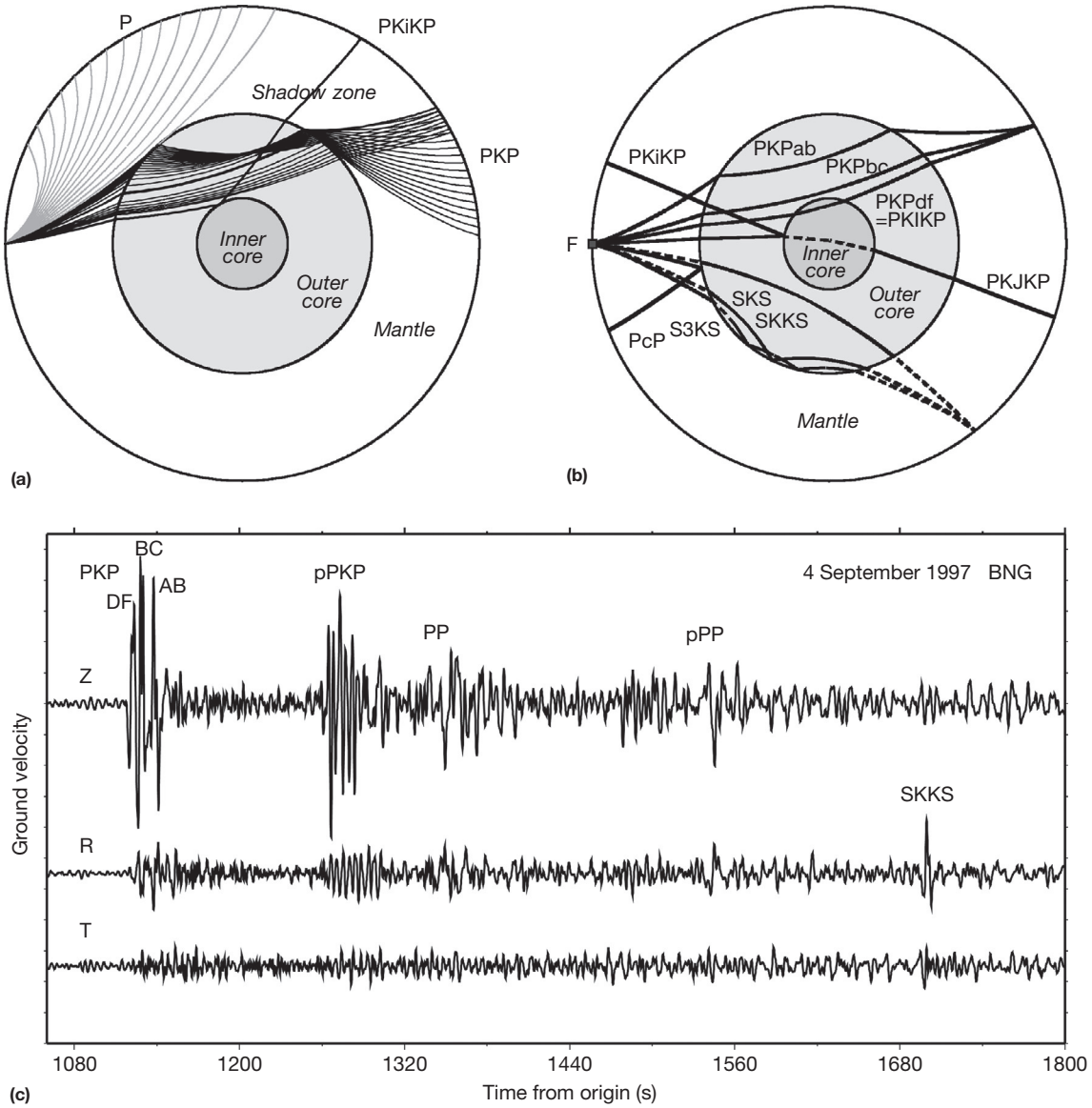

Figure 1 (a) Shadow zone of the core, due to the P-wave velocity decrease from the mantle to outer core, and PKiKP ray reflected at the inner core boundary, at the origin of the discovery of the inner core. (b) Paths of the main core phases inside the Earth propagating as P-waves (full lines) or S-waves (dashed lines). (c) Example of data: the first 11 min record of the Fiji islands, 04 September 1997 event (magnitude $M_b = 6.3$, depth = 621 km), at the Geoscope broadband station BNG (Bangui, Central African Republic), at distance 151°. Three components: Z-vertical, R-radial (in the ray direction), and T-transverse. Note the three phases of PKP on the vertical component, the pPKP phases first reflected at the Earth surface, and the SKKS phase on the radial component. The other phases are mantle phases. Courtesy of E. Stutzmann.

ascribed this phase to a P-wave reflected at an unknown discontinuity at a depth of about 5000 km, the ICB. A physical argument in favor of inner core rigidity is given by Jacobs (1953), who showed that the increase with pressure (thus with depth) of the melting point of iron must result in a phase change from liquid to solid at ICB conditions. An indirect proof of the inner core rigidity is given by the periods of the free oscillations of the Earth that are excited after large earthquakes and that are sensitive to the elastic properties of the deep Earth (Dziewonski and Gilbert, 1971).

Table 1 summarizes the main physical parameters of the core. Elastic parameters are taken from two global Earth models that are widely used as reference, PREM (Dziewonski and Anderson, 1981) and ak135 (Kennett et al., 1995). The temperature is the most poorly defined parameter, as it depends on the composition of the core, which is still debated. In particular, the presence of light elements may decrease the melting temperature of iron by 500–1000 °K (Poirier and Shankland, 1993), depending on their nature and concentration.

1.23.3 Investigation Tools

Among the various tools used to infer the core structure and properties, seismology is certainly the most powerful. Seismic waves allow us to obtain very precise values of the elastic parameters; to image lateral heterogeneities in velocities, anisotropy, and attenuation; and even to seek time variations, induced, for example, by a possible inner core rotation. However, the interpretation of the images obtained by seismology relies strongly on the results of mineral physics at high pressure and high temperature. Another important information is given by the Earth's rotation, in particular nutations and length of day, which are sensitive to the Earth's shape and stratification. The analysis of the magnetic field and its temporal variations give information on the convective motions in the liquid core, which will not be considered here (see Volume 8).

1.23.3.1 Body-Wave Seismology: The Core Phases

Core studies are based on travel times and amplitudes of the different phases sampling the core (compressional waves, shear waves, and combinations of both) and increasingly on whole waveform modeling (see Chapters 1.06 and 1.07). The worldwide digital broadband stations are the main source of waveform data. For travel times, values reported in the bulletins of the International Seismological Centre (ISC) or in derived improved catalogs (EHB file; Engdahl et al., 1998) are also used. For these data, the large amount of values collected since 1964, combined with statistical analyses, compensates for the uneven quality of single values. Finally, for some phases with a very low energy, stacking of records collected at arrays is necessary.

There are three particularities of core phases:

- S-waves, which is are shear waves, do not propagate inside the liquid core. Thus, the liquid core may be investigated only through P-waves.
- The waves sampling the core also travel twice through the mantle and crust, at station side and at source side. The crust and the base of the mantle, the so-called D″ layer, are highly heterogeneous, as well as the upper mantle in most of the source regions, because of the dipping slabs associated with subduction zones. Each time it is possible, it is thus convenient to use differential travel times between neighboring phases, which partly remove the perturbing contributions of the mantle and crust and mislocation and clock errors. In particular, the phase PKP(DF), also called PKIKP, which samples the inner core, is often compared to PKP (BC), a nearby phase that has its turning point at the base of the liquid core and has nearly the same waveform. It may also be compared to PKP(AB), which is more distant, more

Table 1 Main physical parameters for the Earth's core and the main discontinuities, from PREM at 1 s period (Dziewonski and Anderson, 1981), except for hydrostatic equilibrium ellipticity (Bullen and Haddon, 1973), and for temperatures

	Radius (km)	*Depth (km)*	V_P *(km s^{-1})*	V_S *(km s^{-1})*	*Density (g cm^{-3})*	*Pressure (GPa)*	*Temperature (°K)*	*Gravity (m s^{-2})*	*Ellipticity*
Crust and	6371	0	5.80	3.20	2.60	0	300	9.81	1/298.3
mantle	*6371*	*0*	*5.80*	*3.46*					
Silicates of Fe,	3480	2891	13.72	7.26	5.57	140	4100	10.7	1/392.7
Mg	*3479.5*	*2891.5*	*13.66*	*7.28*			(3700–4200)		
Core–mantle boundary (CMB)									
Liquid core	3480	2891	8.06	0	9.90	140	4100	10.7	1/392.7
Iron + light	*3479.5*	*2891.5*	*8.00*	*0*			(3700–4200)		
elements	1221.5	5149.5	10.36	0	12.17	330	5500	4.4	1/411
	1217.5	*5153.5*	*10.29*	*0*			(4600–5700)		
Inner core boundary (ICB)									
Inner core	1221.5	5149.5	11.03	3.50	12.76	330	5500	4.4	1/411
Almost pure	*1217.5*	*5153.5*	*11.04*	*3.50*			(4600–5700)		
iron	0	6371	11.26	3.67	13.09	360	5800	0	0
	0	*6371*	*11.26*	*3.67*			(5000–6000)		

Values in italics, velocity values for model ak135 (Kennett et al., 1995); temperatures from Chapter 9.08 and from Hirose K, Labrosse S, and Hernlund J (2013) Composition and state of the core. *Annual Review of Earth and Planetary Sciences* 41: 25.1–25.35.

affected by D″ heterogeneities, which differs from PKP(DF) by a Hilbert transform (Choy and Richards, 1975), but which is the simplest reference phase at large distance. These three PKP phases form a triplication in the PKP travel time curves as a function of distance.

– Because of their long path through the Earth, core phases have large Fresnel zones inside the core. For example, a PKP(DF) wave of 2 s period samples a tube about 500 km wide at its turning point, which is quite large compared to the inner core radius of 1220 km (Calvet et al., 2006; Figure 2). Thus, PKP(DF) returns a smeared image of the inner core.

A list of the main core phases and their use for core studies are given in Table 2. Their paths inside the Earth are shown in Figure 1(b), and an example of record is shown in Figure 1(c). Some of the paths are purely P-waves, with refractions or reflections at the core boundaries (PKP, PKKP, etc.); others are a combination of S- and P-waves, such as SKS, which propagates as S-wave in the mantle, or PKJKP, which propagates as S-wave inside the inner core.

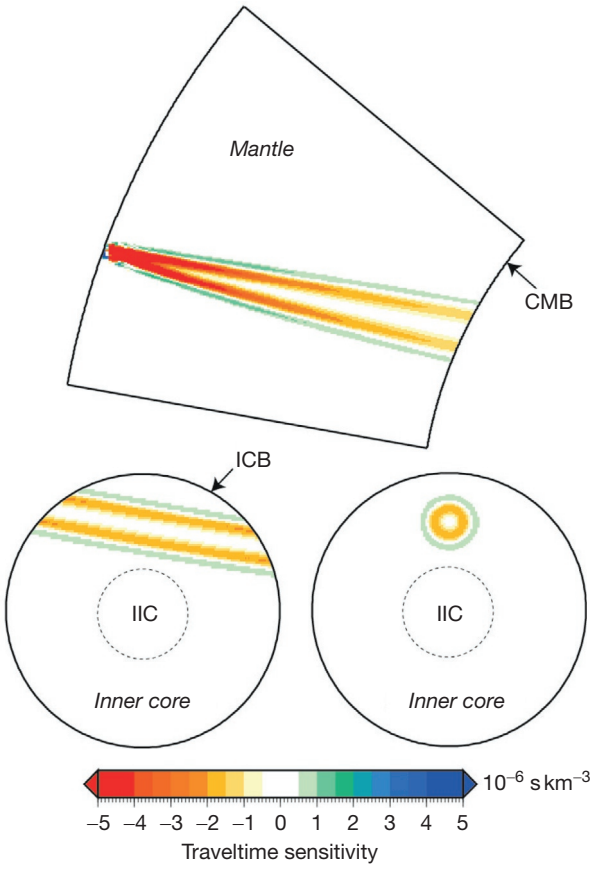

Figure 2 Travel time sensitivity kernel of PKP(DF) at 2 s period and 160° epicentral distance, giving the sensitivity of travel time to structure. (Top) Fresnel zone in the mantle along the ray. (Bottom) Fresnel zone in the inner core along the ray and perpendicular to the ray at its turning point. CMB, core–mantle boundary; ICB, inner core boundary; ICC, innermost inner core (see Section 1.23.7.2.2.3). Note the sensitivity of the PKP(DF) ray to the upper mantle structure and the large size of the Fresnel zone in the inner core, which will smear the images of small-scale heterogeneities or sharp discontinuities.

1.23.3.2 Normal Modes

The periods and amplitudes of free oscillations (or normal modes) allow us to retrieve the mean elastic parameters, density, and attenuation as a function of radius and their long wavelength heterogeneities (see Chapters 1.03 and 1.04). They avoid the problem of sparse sampling due to body waves. The splitting of the modes in multiplets gives information on the anisotropy, once the contributions of the Earth's rotation and ellipticity are corrected (e.g., Durek and Romanowicz, 1999; Dziewonski and Gilbert, 1971; Irving and Deuss, 2011a; Laske and Masters, 2003; Tromp, 1993). Modes are mostly sensitive to the even part of Earth structure. Thus, for example, a possible degree-one (hemispherical) pattern will be difficult to detect, unless mode coupling is considered (Irving et al., 2009). Moreover, only a limited number of modes have significant energy in the core, still fewer in the inner core, and mode energy decreases to zero at the Earth's center. Very large earthquakes are thus required to observe inner core-sensitive modes.

Normal modes are however crucial for core studies, as they allow us to obtain S-velocity and density (Kennett, 1998; Masters, 1979; Masters and Gubbins, 2003), which are very difficult to obtain from body waves. Moreover, they sample the low-frequency part of the spectrum, which is not accessible to body waves. Because of the fluidity of the core, only spheroidal modes are considered.

Figure 3 gives the energy in compression, shear, and density as a function of radius for various core-sensitive modes. The energy in the inner core remains small compared to that in the mantle and liquid core; it is thus necessary to combine data sensitive to different depths to reduce the influence of the mantle. The ability of modes to resolve sharp discontinuities remains however very poor.

1.23.3.3 High-Pressure Physics

High-pressure physics provides essential information for deriving the chemical, mineralogical, and textural structure of the Earth from seismic observations (see Volume 2). For example, the knowledge of the crystal structure of iron alloy is necessary for modeling seismic anisotropy in the inner core and for proposing models of core dynamics. Materials at core conditions may be explored either from laboratory experiments or from theoretical computations. Only few experiments in diamond anvil cells have reached the 360 GPa pressure present at the Earth's center. Core conditions are more easily reproduced by shock-wave experiments even if the temperature remains difficult to estimate. Computations based on first-principle molecular dynamics simulations, or ab initio computations, provide an alternative for simulating core conditions. These methods allow us to predict almost all the parameters of core materials (phase diagram of iron alloy, melting temperature, rheology, elasticity, etc.). However, the results depend on the approximations made and on the input parameters, for example, the nature and the amount of light elements included in the iron alloy.

Table 2 Main body waves sampling the core

Phase name	*Path*	*Use and peculiarities*
PKP(DF) = PKPdf = PKIKP	P propagating through the inner core	Inner core structure and anisotropy
PKP(BC) = PKPbc	P turning at the base of the liquid core	Liquid core structure Reference phase for PKP(DF) at distances 149–155°
PKP(AB) = PKPab	P turning in the middle of the liquid core	D″ structure Reference phase (poor) for PKP(DF) at large distance
PKKP = P2KP, P*n*KP	P with ($n-1$) underside reflections at CMB	Three branches (DF, BC, AB), difficult to observe CMB topography P*n*KP(BC): structure of the liquid core
PcP, ScS, PcS, ScP	P or S reflected as P or S at CMB (upperside reflection)	D″ structure CMB topography PcP: reference phase for PKiKP
PKiKP	P reflected at ICB (upperside reflection)	Topography and scatterers at ICB, density and S-velocity jump at ICB Difficult to observe at short distance
PKJKP	S through the inner core, P elsewhere	S-structure of the inner core Not directly observable
SKS, S*m*KS	S in the mantle, propagating as P in the liquid core ($m-1$) underside reflections at CMB	D″ structure Structure of the uppermost liquid core

CMB, core–mantle boundary; ICB, inner core boundary.

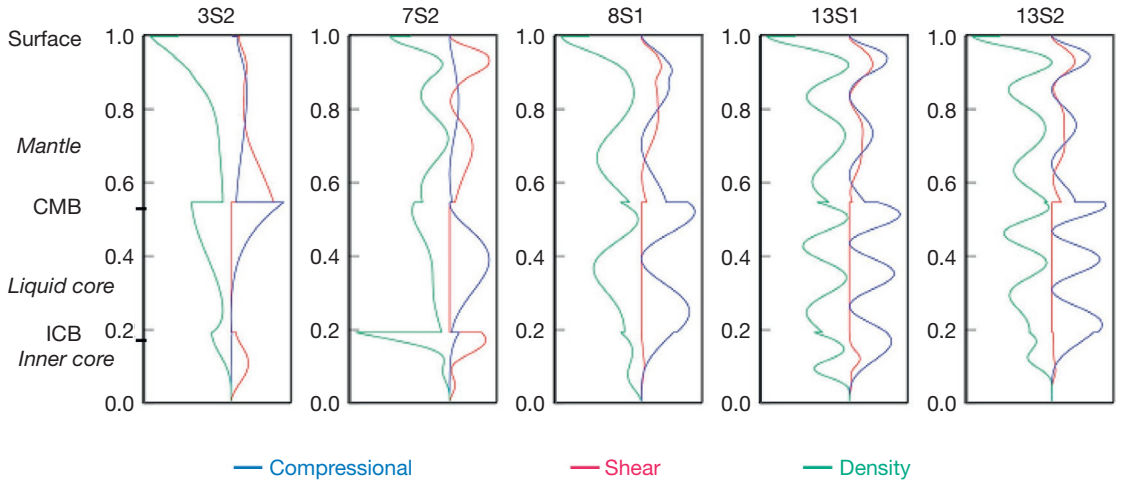

Figure 3 Sensitivity kernels for some core-sensitive modes as a function of radius, for a 1D Earth model (no lateral heterogeneity). Blue lines are for κ (compressional energy), red lines for μ (shear energy; note that it is zero in the fluid outer core), and green lines for density. CMB, core–mantle boundary; ICB, inner core boundary. Courtesy of G. Laske.

1.23.4 Radial Structure of the Core in Global Earth Models

The first accurate core models were derived from travel times and amplitudes of PKP and PKKP waves, from natural earthquakes, and also from nuclear explosions, which provide sources outside subduction zones. S*m*KS waves were used to constrain the upper part of the liquid core, where no PKP wave has its turning point. These models have given with a good precision the radii of the outer core and inner core and the mean velocity profiles and quality factors throughout the core (see references in Souriau and Poupinet, 1991). However, some of these models present artifacts, either because D″ heterogeneities were unmodeled or because PKP precursors, which are due to scatterers at the base of the mantle (Cleary and Haddon, 1972), were erroneously ascribed to a liquid core discontinuity (e.g., Bolt, 1962). This shows the importance of considering whole Earth inversion to obtain reliable reference core models (see **Chapter 1.01**). We will thus consider only the two global models, PREM (Dziewonski and Anderson, 1981) and ak135 (Kennett et al., 1995), which are the most commonly used (**Table 1**). Through this chapter, we will focus on the perturbations to these models inferred from the analyses of specific core phases and normal modes. Several other radial models are also convenient as reference models, for example, SP6 (Morelli and Dziewonski, 1993), IASP91 (Kennett and Engdahl, 1991), and ak135-f (Montagner and Kennett, 1995), derived from ak135 with the addition of density and

shear quality factor. They all exhibit nearly the same features and differ from each other by $<0.5\%$.

PREM (Dziewonski and Anderson, 1981; **Table 1**) was constructed using a combination of body waves and normal modes, thus allowing the authors to obtain a model not only in P- and S-velocities but also in density. The model is compatible with the mass and moment of inertia of the Earth. Moreover, a constraint on stable stratification was introduced a priori in the model before inversion, that is, the Adams–Williamson equation must be satisfied both in the liquid core and in the inner core, each of them assumed to be homogeneous. The final model does not depart significantly from this constraint, except perhaps at the very base of the liquid core. However, some models departing from this stability condition and compatible with normal mode data may also be found (Kennett, 1998).

Model ak135 (Kennett et al., 1995) is constructed from body-wave data only and is right now the best P-wave model inside the core. Its departure from PREM remains small (**Table 1**). ak135 has relatively low velocities at the top of the core but is slightly faster than PREM in the middle of the core. The main difference compared to PREM is a reduced velocity gradient at the base of the liquid core. The P-velocity jump at the ICB is larger in ak135 ($0.75\ \mathrm{km\ s^{-1}}$ instead of $0.67\ \mathrm{km\ s^{-1}}$), a value that may have implications for the percentage and nature of the light elements in the inner core. A comparison of the two models inside the core is shown in **Figure 4**.

It is important to draw attention on several particularities of the velocity profiles in the core. First, the upper part of the liquid core corresponds to a low P-velocity zone with respect to the mantle. This is at the origin of the refraction of P-wave to large distance when it encounters the CMB, giving the so-called shadow zone of the core (**Figure 1(a)** and **5**). The increase of P-velocity with depth bends the ray when its incidence angle decreases, leading to an emergence at shorter distance. This results in a triplication in the PKP travel time curve, each of the branches AB, BC, and DF sampling a different depth range in the core: AB corresponds to a turning point of the ray in the middle of the liquid core, BC at the base of the liquid core, and DF inside the inner core. The three PKP phases coexist in a small distance range between 145° and 155° (**Figure 5**). A second particularity of the velocity profile is that the S-velocity at the base of the mantle is nearly equal to the P-velocity at the top of the liquid core. Thus, the SKS wave (traveling as S in the mantle and P in the liquid core) is not strongly deflected at the CMB (**Figure 1(b)**) and may have its turning point in the uppermost liquid core. Finally, the velocity inside the inner core is nearly constant; thus, the rays are nearly straight. Note also the high Poisson's ratio in the inner core (0.44) compared to that of the mantle (0.26–0.30), which is a characteristic of metals.

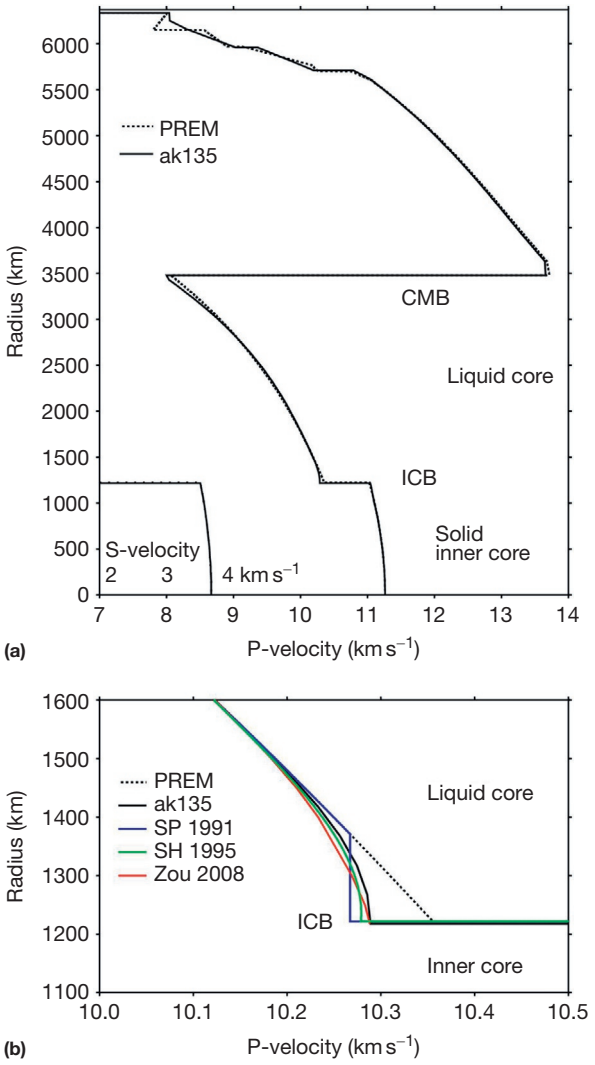

Figure 4 (a) Comparison of the P-velocities for the two global Earth models, PREM (Dziewonski and Anderson, 1981) and ak135 (Kennett et al., 1995). Also shown is the S-velocity model in the inner core (note the different scale). (b) Comparison of the velocity profiles at the base of the liquid core for PREM and ak135 and for three other specific models, Souriau and Poupinet (1991), Song and Helmberger (1995a), and Zou et al. (2008), showing the presence of a low velocity gradient.

1.23.5 The Major Discontinuities

1.23.5.1 The Core–Mantle Boundary

The CMB is the strongest discontinuity in the Earth, with a density jump of $4.3 \times 10^3\ \mathrm{kg\ m^{-3}}$, about 1.5 times larger than the density jump between the Earth's surface and atmosphere. This explains its very important role in Earth dynamics, in particular if a topography is present or if the liquid core has a high viscosity at CMB (see **Chapter 3.10**). The coupling between the core and mantle depends on amplitudes and wavelengths of the CMB topography and influences the Earth's rotation. This topography is induced by mantle dynamics, which is driven by both thermal and chemical heterogeneities (e.g., Defraigne et al., 1996; Forte et al., 1995; Greff-Lefftz and Legros, 1996; Lassak et al., 2010). Recent models predict that the amplitudes generally stay in the range ± 5 km, with a spectrum predominantly at long wavelengths (Lassak et al., 2010). The CMB is also a place where thermal, chemical, and electromagnetic interactions occur between the mantle and core (see **Chapters 7.11**, **8.08**, and **8.09**).

From the seismological point of view, the CMB appears as a first-order discontinuity. It is surrounded by the D″ layer, a

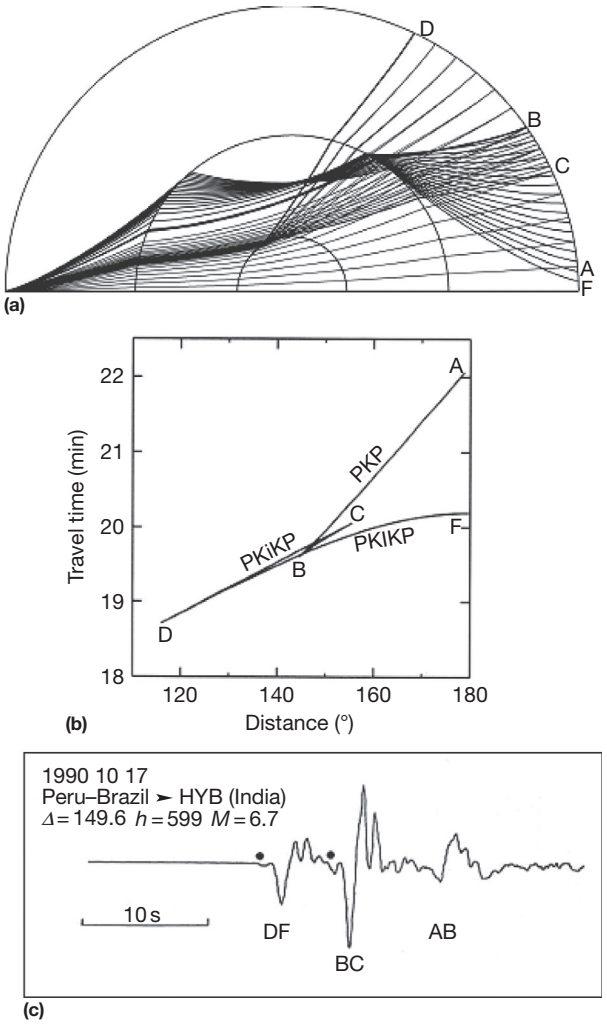

Figure 5 The PKP triplication. (a) Ray paths inside the Earth; (b) PKP travel time curve showing the triplication near 145° and the coexistence of the three PKP phases between 145° and 155°; (c) example of a deep Peru–Brazil event (depth = 599 km) recorded at the Geoscope broadband station HYB (Hyderabad, India), at distance 149.6°. Note the shape similarity between PKP(DF) and PKP(BC), whereas PKP(AB) is the Hilbert transform of PKP(BC).

very heterogeneous layer at the base of the mantle. Large low shear-wave velocity provinces corresponding to compositional heterogeneities are responsible for a strong degree two in the heterogeneity pattern of D″, but a high level of short wavelength heterogeneities is also present (see **Chapters 1.22** and **1.24**). This complex structure of D″ is the strongest difficulty to overcome for the seismological investigation of the CMB.

1.23.5.1.1 The topography of the CMB

The dynamic ellipticity may be obtained from the Earth nutations, which suggest an extra flattening (decrease of polar minus equatorial radius) of about 300–500 m, depending on the importance of the magnetic coupling at the CMB (Gwinn et al., 1986; Mathews et al., 2002). All the other results come either from modeling of mantle dynamics (see **Chapters 1.27** and **7.11**) or from seismology. Seismological results mostly rely on the analysis of travel times and amplitudes of waves reflected at the CMB or transmitted through the CMB (**Table 2**). The data are generally from bulletins. They lead to poorly consistent results, depending on the phases used and on the inverted parameters (Creager and Jordan, 1986; Morelli and Dziewonski, 1987; Rodgers and Wahr, 1993; Obayashi and Fukao, 1997; see references for other early studies in Sze and Van der Hilst, 2003). A major difficulty is the strong trade-off between D″ heterogeneities and CMB topography; it is thus important to include these two structures in the inversion of the data (e.g., Doornbos and Hilton, 1989). Even so, it is difficult to separate these two contributions. Mantle heterogeneities may also be accounted for by coupling mantle dynamics with seismological information (Soldati et al., 2012); this requires strong assumptions on the nature (thermal or chemical) of mantle heterogeneities and on mantle viscosity. Normal modes give an independent approach to the problem, but they allow us to resolve the even part of the topography only, and the trade-off with mantle heterogeneities is again strong (Koelemeijer et al., 2012; Li et al., 1991).

Studies to date propose topographic maps with amplitudes ranging from about 2 to 10 km, for wavelengths generally larger than 4000 km. They are very different from one model to the other. Normal modes give an upper limit of 5 km (Koelemeijer et al., 2012). For body-wave analyses, important biases may result from the existence of unsampled regions at the CMB surface (Pulliam and Stark, 1993). Moreover, simulations show the great difficulty to map both D″ heterogeneities and CMB topography with the presently available data (Garcia and Souriau, 2000a; Sze and Van der Hilst, 2003). A stochastic analysis of residuals of core phases shows that 95% of the CMB topography is in the range $\pm \sim 1.5$ km for characteristic lengths larger than 1200 km (Garcia and Souriau, 2000a). Similar values (± 1.75 km) are obtained in three regions around the Pacific (Koper et al., 2003). This is consistent with the most recent maps obtained at a worldwide scale (Sze and Van der Hilst, 2003), which found a peak-to-peak amplitude of about 3 km.

Short wavelength undulations responsible for wave scattering are also probably present (Rost and Revenaugh, 2004), but they must have very small amplitudes, because of the difficulty to support dynamically such heavy anomalies. They are difficult to quantify, because of the complicated signature they have in both travel times and amplitudes, as revealed by experimental and theoretical models (Emmerich, 1993; Kampfman and Müller, 1989; Menke, 1986; Rekdal and Doornbos, 1992). PcP amplitudes limit this topography to a few hundred meters in the wavelength range 2–50 km (Menke, 1986); PKKP precursors suggest topographic highs of the order of 300 m with correlation lengths of about 10 km (Earle and Shearer, 1997; Shearer et al., 1998) (see **Chapter 1.24**).

1.23.5.2 The Inner Core Boundary

This boundary is essential to understand the growing mechanism of the inner core and the thermal, chemical, and mechanical interactions between liquid and solid cores. Several models of growth are proposed, implying either a dendritic growth at the inner core surface (Bergman et al., 2003) or a slurry layer made of unconnected particles that crystallize above the ICB (Loper and Roberts, 1981; Shimizu et al., 2005). The prevailing mechanism will depend on the iron alloy present at the base of

the liquid core (Hirose et al., 2013) and on the thermodynamic conditions. Seismic data may help specify this mechanism. For example, the velocity and density contrasts at the ICB are key parameters for specifying the amount of light elements in the core and to detect partial melting at the ICB.

From the geodynamic point of view, the ICB has only a limited influence, as it corresponds to a weaker density contrast and to a smaller radius than the CMB. It has, however, an impact on the Slichter mode, a translation mode of the inner core inside the fluid whose period of about 5 h is very sensitive to the density contrast and liquid core viscosity at the ICB (Crossley et al., 1992; Rosat et al., 2006).

Seismic waveforms indicate that the ICB can generally be considered as a first-order discontinuity, <2 km thick (Cummins and Johnson, 1988a; Kawakatsu, 2006). This is consistent with thermodynamic considerations: although the uppermost inner core may incorporate fluid inclusions when it forms, it is likely to collapse under its own weight, the unconsolidated material having a thickness probably smaller than 1 km (Deguen et al., 2007).

1.23.5.2.1 The topography at ICB

The topography at ICB is certainly very weak and present at long wavelength only: first, because iron is at its melting point, thus freezing or melting will erase any topography as soon as the liquid core may transport latent heat, and, second, because the inner core has a low viscosity, probably in the range 10^{11}–10^{22} Pa s (Buffett, 1997; Deguen, 2012). Seismic waves reflected at different latitudes at the ICB show that the ellipticity is consistent with the equilibrium figure in a rotating Earth (Souriau and Souriau, 1989). An ICB topography could be induced by the gravimetric forcing of the mantle and inner core heterogeneities, with in addition the dynamic response to a possible convection inside the inner core. Mantle loading and inner core loading give each a stable topography of the order of 100 m peak to peak (Defraigne et al., 1996); thus, it could not be detected by seismological methods. However, local topographies of about 100 m to more than 10 km, with horizontal extension of a few kilometers, are reported from observations of waves reflected at the ICB by several authors (Cao et al., 2007; Dai et al., 2012; Song and Dai, 2008). If these observations are sound, they may indicate a high viscosity at the top of the inner core or the presence, at least at some places, of solid inclusions at the base of the liquid core forming a slurry boundary.

1.23.5.2.2 The density jump at ICB and its implications

At vertical incidence, the impedance contrast of a discontinuity depends primarily on its density contrast. Thus, the density jump at the ICB, $\Delta\rho_{ICB}$, may be directly obtained from the amplitude of the PKiKP waves reflected normally at the ICB. It is generally referred to the amplitude of the PcP waves reflected at the CMB, provided that the velocity and density contrasts at the CMB are known (Bolt and Qamar, 1970). As PKiKP has small amplitude at vertical incidence, stacking of several records is generally necessary to enhance the signal. Away from vertical incidence, there is a strong trade-off between density contrast, shear velocity contrast, and attenuation at the top of the inner core, as shown from waveform modeling of PKP (Cummins and Johnson, 1988b).

Density jump at the ICB ranging from 0.2 to 1.4 g cm^{-3} has been obtained from the amplitude ratios PKiKP/PcP (Figure 6) or PKiKP/P, assuming that the density contrast at the CMB has PREM's value (Cao and Romanowicz, 2004a; Koper and Dombrovskaya, 2005; Koper and Pyle, 2004; Shearer and Masters, 1990; Souriau and Souriau, 1989; Tkalčić et al., 2009). On the other hand, the data at large epicentral distances seem to require a low shear velocity jump at the ICB (2.0–2.5 km s^{-1}) compared to PREM (Cao and Romanowicz, 2004a; Koper and Pyle, 2004). These measurements are however very scattered, and this variability may reflect the sensitivity of the data to mantle structure and CMB topography, which induce wave focusing and defocusing (Leyton and Koper, 2007a). It could also reflect a variable density contrast at the CMB, which affects the reference phase PcP (Tkalčić et al., 2009), or lateral heterogeneities at the inner core surface (Krasnoshchekov et al., 2005).

Normal modes give mean values of $\Delta\rho_{ICB}$ of 0.6–1.0 g cm^{-3} (Kennett, 1998; Masters and Gubbins, 2003). Although these values correspond to a broader depth range than body waves on both ICB sides, due to mode resolution, they are globally compatible with the values obtained in the most recent body-wave studies.

The density contrast inferred from seismology is significantly too high to be explained solely by the change in volume due to a phase transition (Alfè et al., 2003). It requires chemical partitioning during crystallization, with a depletion of the inner core in light elements compared to the liquid core.

1.23.6 The Liquid Outer Core

1.23.6.1 The Main Questions Relative to Liquid Core Structure

The comparison of seismological results with high-pressure experiments and theoretical computations has shown that

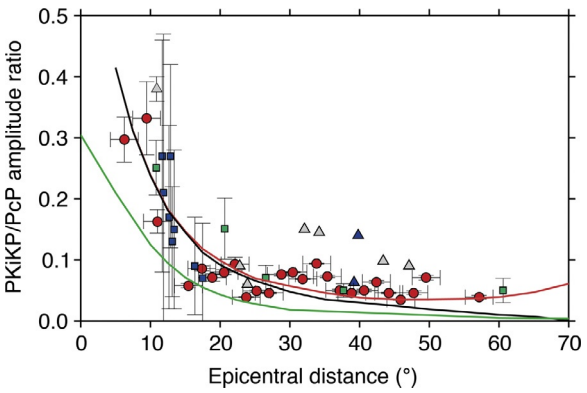

Figure 6 The amplitude ratio of the two phases PKiKP (reflected at inner core boundary ICB) and PcP (reflected at core–mantle boundary) as a function of distance, for the determination of the density contrast $\delta\rho$ and S-velocity contrast δv_S at ICB. Symbols are experimental values. Gray triangles, early results compiled by Souriau and Souriau (1989); blue triangles, Shearer and Masters (1990) (data with identified PKiKP phase); green squares, best data of Cao and Romanowicz (2004a); red dots, binned values of Koper and Pyle (2004) (horizontal bars correspond to the binning intervals); blue squares, Tkalčić et al. (2009). Curves, theoretical values; black, PREM ($\delta\rho = 0.6$ g cm^{-3}, $\delta v_S = 3.5$ km s^{-1}); green, same as PREM with $\delta\rho = 0$, showing the need for depletion in light elements during crystallization; red, same as PREM with $\delta v_S = 2.5$ km s^{-1}, suggesting a v_S decrease in the uppermost inner core.

the outer liquid core is less dense than the pure molten iron at the same conditions of temperature and pressure, indicating the presence of light elements in the core, in an amount of about 10% by weight (Birch, 1964; Jephcoat and Olson, 1987; Poirier, 1994). Many candidates are possible. Sulfur has a great solubility inside liquid iron at core conditions; it is thus a possible candidate, but other elements such as O, N, Si, and K are likely to be present (Alfè et al., 2003; Andrault et al., 2009; Badro et al., 2007; Hirose et al., 2013; Poirier, 1994). The radioactive isotope ^{40}K, if present in the core, will be an additional source of energy to power the Earth dynamo. The presence of Ni (which has a higher density than Fe) in a proportion of about 4% is far from compensating the density decrease due to light elements (see **Chapters 2.06** and **8.02** for more details about the chemical state of the outer core).

The main questions relative to the fluid core concern its possible radial inhomogeneity, due in particular to the presence of these light elements. They are released at the ICB when the liquid iron alloy crystallizes, may migrate upward, and form a distinct alloy layer beneath the CMB. A stratification or a distinct layer at the top of the core is thus possible; it is predicted by thermodynamic models of core evolution (Buffett and Seagle, 2010; Lister and Buffett, 1998). It may influence the core–mantle coupling with consequences for Earth dynamics, nutations, and length of day and for the magnetic field (see **Chapter 3.10**). It may also give constraints on the nature of the light elements (Helffrich and Kaneshima, 2004). On the other hand, a dense layer at the base of the liquid core, due to heavy alloys, could bring information on the crystallization process of the inner core. A stratification may also result in variations of the thermal conductivity with depth. It is thus important to go in more details in the radial core structure. The periods of free oscillations indicate that the outer core is not strongly stratified (Masters, 1979). This is confirmed by the velocity profiles in global Earth models, which indicate radial homogeneity, except close to the core boundaries. If stratification is present, it will thus concern primarily the boundaries.

Lateral heterogeneities inside the liquid core are less probable, as an active convection is made possible by the low viscosity of the liquid alloy, comparable to that of water at the Earth surface ($\eta = 6 \times 10^{-3}$ Pa s, Poirier, 1988), or possibly slightly higher at the core boundary (Koot et al., 2010; Palmer and Smylie, 2005; Smylie, 1999; see also the review in Cormier et al., 2011). However, fluid motions in a rotating fluid sphere are organized in cylinders with axis parallel to the Earth's rotation axis (ERA) (Busse, 1975). The structures inside the cylinder tangent to the inner core are thus partly insulated from the fluid outside this tangent cylinder, being perhaps able to carry material with distinct properties. Sedimentation of a different material beneath the polar caps or the equatorial bulge may also be favored by the rotation.

The following sections present the seismological approach to these questions.

1.23.6.2 The Stratification at the Base of the Liquid Core

The propagation time of the PKP(BC) wave, which becomes diffracted along the ICB at large distance (giving the PKP(C_{diff}) wave), gives direct information on the structure of the lowermost 150 km of the liquid core. The velocities appear significantly lower than those of PREM, which roughly correspond to the adiabatic gradient (Souriau and Poupinet, 1991). This has been confirmed from waveform modeling of short-period records (Song and Helmberger, 1992, 1995a) and from other PKP(C_{diff}) observations (Zou et al., 2008). The data are well explained by a low velocity gradient in the lower 100–150 km at the base of the liquid core, where the velocity becomes nearly constant (**Figure 4(b)**). This low velocity gradient layer is sometimes improperly called the F-layer, in reference to a denomination of Bullen (1940). The anomalously low-amplitude decay of the diffracted waves PKP(C_{diff}) with distance (Song and Helmberger, 1995a; Souriau and Roudil, 1995) is another argument in favor of this low velocity gradient, which acts as a guide for the diffracted waves. However, the amplitude ratios of PKP(C_{diff})/PKP(DF) are close to PREM's predictions (Zou et al., 2008), an observation interpreted as due to either small-scale topography at the ICB or a thin sub-layer of relatively low-quality factor at the very base of the outer core.

A hemispherical pattern has been proposed for the low velocity layer (Yu et al., 2005), but the inner core structure could be responsible for this pattern as well (Cormier et al., 2011). Such a heterogeneity could not be sustained by the liquid unless its viscosity is very high (Cormier et al., 2011). This is not completely excluded: This layer could be a zone of small, nonzero rigidity ($v_S = 0.1$–0.5 km s^{-1}), as revealed by both normal modes (Mochizuki and Ohminato, 1989) and PKiKP waves reflected at the ICB (Cormier, 2009); thus, it could also be a zone of increased viscosity. The free inner core nutations suggest a viscosity of $\sim 10^5$ Pa s (Koot et al., 2010). The Slichter mode would be sensitive to such a layer (Smylie, 1999), but its identification on superconducting gravimeter records is highly controversial (Rosat et al., 2006).

Gubbins et al. (2008) have clearly shown that this low-velocity, high-density layer must be of compositional origin. In a slurry model, freezing and melting occur in this layer, and the P-velocity gradient is caused by a compositional gradient with heavy elements at the bottom. Melting appears necessary to generate this layer. Two mechanisms, which may coexist, have been invoked to produce melting: an inner core translation in the equatorial plane (Alboussière et al., 2010; Monnereau et al., 2010) and the thermal forcing by outer core convection (Gubbins et al., 2011). Alboussière et al. (2010) argue that melting on the inner core hemisphere exposed to pressure decrease during translation will produce a dense iron-rich liquid that spreads at the surface of the inner core. Gubbins et al. (2011) propose that melting occurs in response to heat transport by the outer core flow. This flow is driven by the large lateral variations of heat extraction at the CMB; it induces a large area of melting at the ICB under the Pacific and freezing mainly located under Indonesia.

1.23.6.3 The Stratification at the Top of the Liquid Core

The uppermost third of the core is mostly investigated with the S*m*KS wave, which becomes a whispering wave beneath the CMB for large *m* (*m* up to five has been observed as a distinct phase). Unfortunately, its travel time is strongly affected by the heterogeneities in the D″ layer, an effect that is only imperfectly corrected by the use of differential travel times between successive S*m*KS phases. Waveform modeling of S*m*KS may also be

used (Choy, 1977). Normal modes that sample the CMB region also provide useful information but, as previously said, they have poor depth resolution.

The different results do not lead to a consensus. Several studies implying different methods have proposed the presence of a thin (50–100 km thick) layer with slightly lower velocities at the top of the liquid core, which could correspond to an iron alloy enriched in light elements (Garnero et al., 1993; Helffrich and Kaneshima, 2010; Lay and Young, 1990; Tanaka, 2007). However, some studies fail to identify a distinct layer (Alexandrakis and Eaton, 2010; Helffrich and Kaneshima, 2004), while others detect a layer with increased velocity (Eaton and Kendall, 2006) or large-scale heterogeneities (Tanaka and Hamaguchi, 1993). The resolution of the different methods is, however generally not sufficient to discard the influence of lower mantle heterogeneities. It turns out that a thin uppermost distinct fluid layer is generally not required by the data (Garnero and Lay, 1998; Kohler, 1997).

Finally, the presence of a very thin, conductive, and slightly rigid layer of silicate deposits at the top of the core has been proposed to explain the amplitudes of the Earth nutations (Buffett et al., 2010). Even though normal modes may be compatible with a small amount of shear at the top of the liquid core (Romanowicz and Bréger, 2000), its seismological detection is still questionable (Rost and Revenaugh, 2001).

1.23.6.4 Search for a Three-Dimensional Structure Inside the Liquid Core

Gravitational forcing from the heterogeneities located inside the mantle and inner core (Piersanti et al., 2001; Wahr and de Vries, 1989) and steady-state dynamics must result in a 3D structure inside the fluid core. However, as shown by Stevenson (1987), the liquid core is not able to sustain relative density heterogeneities $\delta\rho/\rho$ larger than 10^{-4}. Assuming that velocity heterogeneities in liquid iron are proportional to density heterogeneities with a proportionality factor of -1 (Stevenson, 1987), the heterogeneities will be much below the level of detection by seismological methods. Despite this theoretical limit, several seismological results propose an outer core structure, that is, a departure from spherical symmetry (after ellipticity correction).

A large-scale aspheric structure in the liquid core is suggested by the splitting of some normal modes, which are difficult to explain by inner core and mantle structure alone (Ritzwoller et al., 1986; Widmer et al., 1992). Pushing to the extreme, it would be possible to explain the splitting of most of the core modes by outer core structure only (Romanowicz and Bréger, 2000), although the favored interpretation, which is more physically acceptable, is inner core anisotropy, as will be seen later.

A search for cylindrical structures related to the magnetohydrodynamic models of the core, such as embedded cylinders parallel to the ERA, has been performed using travel times of SKS and PKP(BC) and normal modes. No evidence of heterogeneity could be firmly established. PKP(BC) shows that P-velocities are identical inside and outside the tangent cylinder (Ohtaki et al., 2012; Souriau et al., 2003b; Yu et al., 2005), a result confirmed by normal mode analyses (Ishii and Dziewonski, 2005). It has also not been possible to detect P-wave anomalies beneath the polar caps nor beneath the equatorial bulge (Souriau et al., 2003b).

1.23.6.5 The Attenuation in the Liquid Core

Measurements of attenuation in the liquid core at high frequency (~1 Hz) are based on the amplitude of the phases P*n*KP reflected $(n-1)$ times under the CMB, with n up to 7 (**Figure 7**). The quality factor for P-waves, Q_α, is larger than 5000–10 000 (Cormier and Richards, 1976; Qamar and Eisenberg, 1974). Slightly lower values ($Q_\alpha = 1600$–7000, depending on frequency) are given by Tanaka and Hamaguchi (1996). Q_α may thus be considered as close to infinity. Such large values are not found elsewhere inside the Earth. Very large values are also obtained from normal mode analyses ($Q_\alpha = 12\,000$, Widmer et al., 1991), suggesting that Q is not strongly frequency-dependent inside the liquid core.

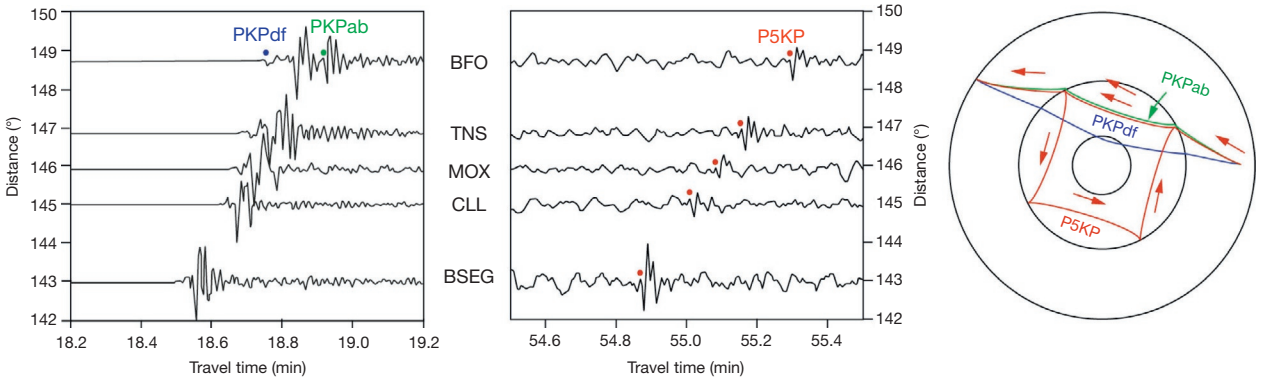

Figure 7 Right: Path of the P5KP wave inside the Earth (red), for a deep event of Fiji Island region (Dec. 18, 2000). The path of the PKP(AB) ray is superimposed (green); also shown is the PKP(DF) ray turning inside the inner core (blue). Left and middle: Waveforms of PKP and P5KP, respectively, recorded at different distances (station codes are between the two figures). The observation of P5KP on single records and its shape similarity with PKP(AB) are all together a proof of the lateral homogeneity of the liquid core, of its low attenuation, of the strong P-wave reflection coefficient underside the core–mantle boundary (which appears as a first-order discontinuity), and of the absence of significant topography at this boundary. Modified from Figure 11.71 of Bormann P, Klinge K, and Wendt S (2002) Chapter 11: Data analysis and seismogram interpretation. In: Bormann P (ed.) *IASPEI New Manual of Seismological Observatory Practice*, vol. 1, 102 pp. Potsdam: GeoForschungsZentrum; © IASPEI, with permission.

1.23.7 The Inner Core: Seismic Velocities

Seismic data have allowed us to establish the rigidity of the inner core, to specify its radial structure, and to detect long wavelength lateral variations. One of its most spectacular physical properties is its anisotropy, present in a large volume of the inner core: waves that propagate parallel to the ERA travel faster than those that propagate parallel to the equatorial plane. The anisotropy inside the inner core is however not uniform, with both radial and lateral variations. A hemispherical heterogeneity, which roughly distinguishes the Eastern and the western hemispheres defined with respect to the origin meridian, destroys the symmetry with respect to ERA. It is a very intriguing feature and a fundamental piece of information to understand how the inner core grows and how the anisotropy is generated.

1.23.7.1 S-Waves and the Rigidity of the Inner Core

Evidence of the rigidity of the inner core and v_S profiles inside the inner core have been mostly obtained by indirect observations. The observed periods of core-sensitive normal modes require rigidity (Dziewonski and Gilbert, 1971). They robustly constrain the mean value of the S-velocity to 3.5–3.6 km s^{-1} (Deuss, 2008; Dziewonski and Gilbert, 1971; Masters, 1979; Suda and Fukao, 1990), close to that of mean PREM. However, normal modes have no sensitivity at the Earth's center. The modeling of the PKP waveforms generally gives lower v_S values beneath the ICB, from nearly 0 (Choy and Cormier, 1983) to 2.5–4.0 km s^{-1} (Cummins and Johnson, 1988b; Häge, 1983; Müller, 1973). Amplitudes of the PKiKP reflected wave also favor a small v_S value at the ICB, of the order of 2–3 km s^{-1} (Cao and Romanowicz, 2004a; Koper and Dombrovskaya, 2005; Koper and Pyle, 2004; Shearer and Masters, 1990). Generally, these values are significantly lower than those given in global Earth models. Their compatibility with normal mode results implies the existence of a strong shear velocity gradient in the uppermost 200–300 km of the inner core (Cao and Romanowicz, 2004a; Choy and Cormier, 1983; Häge, 1983).

A direct evidence of the rigidity of the inner core relies on the detection of the phase PKJKP, which propagates as an S-wave inside the inner core and as a P-wave outside. Because of the very low amplitude of this phase, due to the strong shear-wave attenuation in the inner core, to the poor P- to S-wave conversion factor at the ICB, and to S-wave splitting due to anisotropy, there is no hope to observe PKJKP on single records. Stacking of several records is thus necessary to enhance the signal and even so is the success quite uncertain (Doornbos, 1974; Shearer et al., 2011). Optimal conditions are required for stacking, in particular, the appropriate phase velocity and distance and the appropriate frequency domain. This constitutes the major difficulty, because these conditions are poorly known. The distance at which PKJKP will have its maximum amplitude depends on the velocity and density contrasts at the ICB and on the S-velocity profile inside the inner core, which are not well known. In the worst case, if the S-velocity is close to zero at the top of the inner core (Choy and Cormier, 1983; Cormier et al., 2011), PKJKP will simply not exist. This may occur if a mushy zone is present at the top of the inner core. The frequency domain where PKJKP is observed is also unknown, although the strong attenuation inside the inner core suggests that it must be better detected on broadband records than on short-period records.

An identification of PKJKP on short-period records is proposed in three studies: Julian et al. (1972) proposed a very low S-velocity of 2.95 km s^{-1} in the inner core, whereas Okal and Cansi (1998) and Wookey and Helffrich (2008) found values close to those proposed in mean Earth models. Studies on broadband data have been conducted by Kawakatsu (1992), Deuss et al. (2000), Cao et al. (2005), and Shearer et al. (2011). Kawakatsu and Shearer et al. failed to observe PKJKP. Deuss et al. obtained a velocity of 3.6 km s^{-1} from the observation of a combination of two other parent phases (pPKJKP + SKJKP). Cao et al. obtained a clear phase arriving 9 s before PREM's predictions, implying that, if this phase is really PKJKP, v_S in the deep inner core must be about 1.5% larger than in PREM, where it is mostly constrained by normal modes sampling the outer part of the inner core. The two models may be reconciled if v_S increases with depth inside the inner core.

Most ab initio calculations on the elastic properties of iron crystals in the inner core display v_S values significantly higher than those inferred from seismology (Deuss, 2008; Vočadlo, 2007). This discrepancy has been used to support the presence of liquid in the inner core, resulting from dendritic solidification (Deguen et al., 2007; Singh et al., 2000; Vočadlo, 2007). Alternative explanations invoke the role of light elements and nickel, the presence of crystal defects that induces low rigidity (Belonoshko et al., 2007), or wave scattering by polycrystalline aggregates, in which wave velocity is decreased compared to that in single crystals (Calvet and Margerin, 2008).

1.23.7.2 The Anisotropy in P-Wave Velocity

The investigation of inner core anisotropy faces two major difficulties: (1) finding rays with various orientations turning in the same region at the same depth (from this point of view, the inner core sampling is very poor) and (2) getting rid of the perturbing contributions of the crust and mantle structures. Polar paths (i.e., paths parallel to ERA) are crucial, but they are rare, with an oversampling of the path from South Sandwich Island events to high-latitude stations, which often appear as anomalous (Tkalčić et al., 2002). In parallel, modeling relies on strong assumptions concerning the characteristics of anisotropy.

1.23.7.2.1 Evidence for anisotropy in P-wave velocity: early studies

The evidence of faster propagation along the polar axis than in the equatorial plane was first reported by Poupinet et al. (1983) from the analysis of the large amount of the PKP(DF) residuals collected by the ISC. This anomaly has been interpreted by Morelli et al. (1986) as due to inner core anisotropy. It is also well observed in the differential travel times of PKP(DF)–PKP(BC) and PKP(DF)–PKP(AB) (**Figure 8**). These observations confirm that the anomaly originates in the inner core, not in the liquid core or in the mantle (e.g., Creager, 1992; Shearer et al., 1988). On the other hand, the anomalous splitting of inner core-sensitive normal modes, which remains after correction for ellipticity and the Earth's rotation, is also well explained by anisotropy (Li et al., 1991; Tromp, 1993;

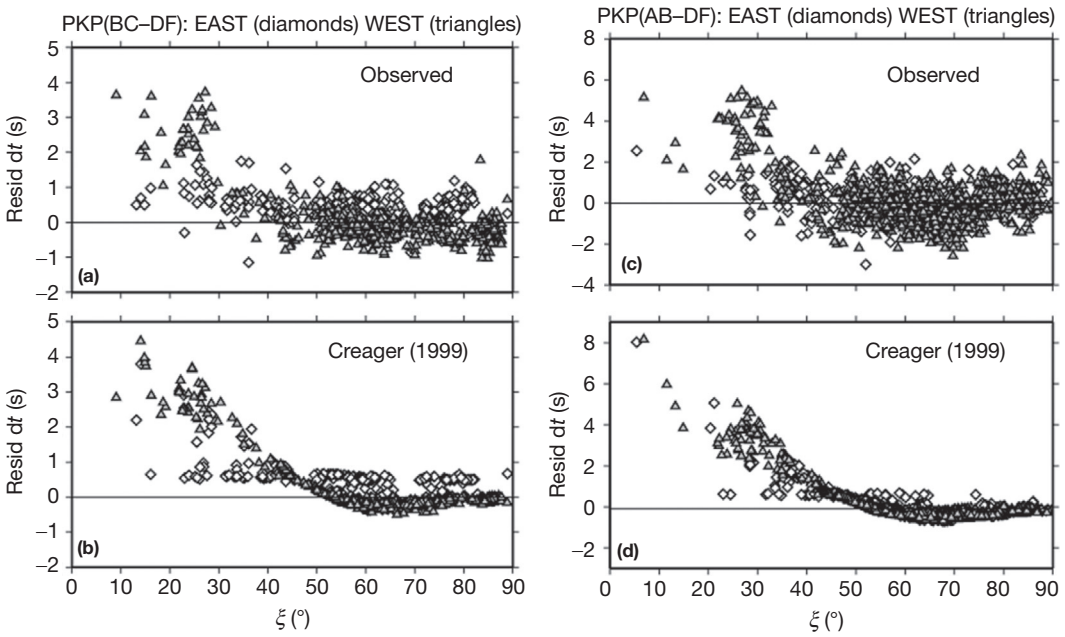

Figure 8 Evidence for anisotropy in the inner core. Differential travel time residuals for PKP(BC)–PKP(DF) (a) and for PKP(AB)–PKP(DF) (c) as a function of the angle ξ of the ray inside the inner core with respect to the Earth's rotation axis, distinguishing quasi-eastern (diamonds) and quasi-western (triangles) hemispheres (see **Section 1.23.7.2.2.2**). The high residuals at low ξ-values reveal that PKP(DF) polar paths are faster than equatorial paths. (b and d) Predictions of a cylindrical anisotropy model (transverse isotropy) by Creager (1999), with different coefficients for the two hemispheres. Reproduced from Romanowicz B, Tkalčić H, and Bréger L (2003) On the origin of complexity in PKP travel time data. In: Dehant V, et al. (eds.) *Core Dynamics*, *Structure and Rotation*. *Geophysical Monograph*, vol. 31, pp. 31–44. Washington, DC: American Geophysical Union.

Woodhouse et al., 1986). The travel time anomaly, after ellipticity correction, may reach up to 6 s for polar paths (Vinnik et al., 1994), compared to a total propagation time of about 1200 s through the Earth, of which about 220 s is through the inner core. Such a P-wave travel time anomaly is very large, compared to those observed for propagation through the mantle, which rarely exceed 2 s. A uniform cylindrical anisotropy (transverse isotropy), with a fast axis parallel to ERA and a level of anisotropy between 1.5% and 4%, explains the general features of the data (e.g., Creager, 1992; McSweeney et al., 1997; Morelli et al., 1986; Shearer, 1994; Song, 1996; Su and Dziewonski, 1995; Vinnik et al., 1994; see also a compilation of models in Ishii et al., 2002b). It is however insufficient to explain all the seismological observations, as a significant non-axisymmetric signal is also present (Su and Dziewonski, 1995) (see Tkalčić and Kennett, 2008, for a review of the first results).

One of the most commonly used expressions for representing inner core cylindrical anisotropy is (Su and Dziewonski, 1995)

$$\delta v_P/v_0 = a_0 + \varepsilon \cos^2\xi + \gamma \sin^2 2\xi \qquad [1]$$

where ξ is the angle between the ray inside the inner core and the symmetry axis. ε represents the P-wave anisotropy, that is, the difference between the P-velocity along the symmetry axis and the velocity perpendicular to it; γ is a mixed term that controls the P-wave propagation at intermediate angles; and a_0 represents a perturbation with respect to the P-velocity v_0 of the reference model. Many other equivalent expressions are also used in the literature (see equivalences in Calvet et al., 2006). The isotropic velocity is defined as the mean of the anisotropic velocity over the whole space (Creager, 1999), and its perturbation with respect to the reference model is given by

$$(\delta v_P/v_0)_{iso} = a_0 + \varepsilon/3 + (8/15)\gamma \qquad [2]$$

As will be seen hereafter, depth dependence and long wavelength variations are present in the anisotropy, thus, in the a_0, ε, γ parameters.

Some studies have proposed that the anisotropic symmetry axis could be slightly tilted with respect to ERA (Creager, 1992; Romanowicz et al., 1996; Su and Dziewonski, 1995). The data are well explained by such models, but the tilt is not required; it may result from the lack of data in some directions (Souriau et al., 1997). The question has also been raised whether the anisotropy could be an artifact due to mantle or liquid core heterogeneities that, because of their geographic distribution, may mimic a polar fast propagation (Bréger et al., 2000a,b; Ishii et al., 2002a; Romanowicz et al., 2003). Such a contribution is probable, but cannot fully explain the observations (Romanowicz and Bréger, 2000; Tkalčić et al., 2002). Anisotropy thus seems to provide the simplest explanation able to reconcile most of the seismological observations. We will specify hereafter its main characteristics.

1.23.7.2.2 Depth dependence of the anisotropy and hemispherical variations

The variation of anisotropy with depth is mostly deduced from the travel time anomalies of PKP(DF) as a function of epicentral distance for different ray orientations with respect to ERA. PKP(DF) is referred to the PKiKP reflected wave for sampling the uppermost 100 km, to PKP(BC) for the depth range 100–500 km, and to PKP(AB) at greater depths (**Figure 5(a)**).

1.23.7.2.2.1 The isotropic layer

There is a general agreement about a low level of P-wave anisotropy (<1%) in the uppermost 50–150 km of the inner core, with even perhaps no anisotropy at all (Creager, 1999, 2000; Garcia and Souriau, 2000b; McSweeney et al., 1997; Ouzounis and Creager, 2001; Shearer, 1994; Song and Helmberger, 1995b, 1998; Waszek and Deuss, 2011). Normal modes do not require this layer; they limit its mean thickness to 150–200 km (Durek and Romanowicz, 1999; Ishii et al., 2002a,b). Irving and Deuss (2011a) show that it is isotropic for both P- and S-waves. Some seismic observations favor a sharp discontinuity between the isotropic layer and the underlying anisotropic structure (Ouzounis and Creager, 2001; Song and Helmberger, 1998; Waszek and Deuss, 2011), but this is still controversial, as waves reflected at this discontinuity are not widely observed, and scattering from small-scale heterogeneities within the inner core may explain these observations as well (Leyton et al., 2005).

A hemispherical heterogeneity in this layer has been clearly identified by Niu and Wen (2001) from PKiKP and PKIKP records, the velocities in the quasi-eastern hemisphere (longitudes 40–180° E) being higher than in the Western one (**Figure 9**). This result reinforces previous sparse observations (Cormier and Choy, 1986; Kaneshima, 1996). It has been confirmed and refined by many other studies, which specify the level of heterogeneity in each hemisphere, the velocity gradient beneath the ICB, the depth to which the isotropic layer extends, and the longitudes of the transition between hemispheres (Cao and Romanowicz, 2004b; Garcia, 2002b; Waszek and Deuss, 2011; Wen and Niu, 2002; Yu and Wen, 2006a). For example, Yu and Wen (2006a) obtain a velocity gradient beneath the ICB that is larger in the quasi-western hemisphere than in the quasi-eastern hemisphere (5.0×10^{-4} and 0.4×10^{-4} (km s^{-1} km^{-1}, respectively), together with a smaller velocity jump at the ICB (0.65 and 0.75 km s^{-1}, respectively). There are significant variations among the different results: Irving and Deuss (2011b) give a difference in isotropic velocity of only 0.2% between the two hemispheres, Niu and Wen (2001) propose a value of 0.8%, Monnereau et al. (2010) obtain a value close to 0.5%, and Tanaka (2012) proposes 1.4% from equatorial paths. This hemispherical difference extends at least down 85 km beneath the ICB (Cao and Romanowicz, 2004b), possibly deeper (Tanaka, 2012; Yu and Wen, 2006a). The total thickness of the isotropic layer is also different for the two hemispheres, of the order of 100 km beneath the western hemisphere, extending deeper (400 km) beneath the Eastern one (Creager, 2000; Garcia and Souriau, 2000b). Monnereau et al. (2010) find a smooth transition between the two hemispheres, a result also supported by data sampling the high southern latitudes (Ohtaki et al., 2012). By contrast, Waszek and Deuss (2011) and Miller et al. (2013) propose sharp boundaries, but the same data may be as well explained by smooth variations in inner core texture from one hemisphere to the other (Geballe et al., 2013).

Heterogeneities in the isotropic layer are certainly present at other scale lengths. A broad, 3% low-velocity layer has been detected at the top 40 km of the inner core beneath equatorial Africa and the Indian Ocean (Stroujkova and Cormier, 2004). Local variations in the velocity at the ICB (Krasnoshchekov et al., 2005) or in the thickness of the isotropic layer (Yu and Wen, 2007) have also been proposed.

1.23.7.2.2.2 The anisotropy down to ~700 km depth

Beneath the isotropic layer, in the depth range 100–700 km for the quasi-western hemisphere and 400–700 km for the quasi-eastern one, anisotropy with fast axis parallel to ERA provides the simplest way to explain the dependence of P-wave velocity to ray angle ξ.

The difference between a strongly anisotropic quasi-western hemisphere and a weakly anisotropic quasi-eastern hemisphere is clearly pointed out by Tanaka and Hamaguchi (1997) from the differential travel times PKP(BC)–PKP(DF) (**Figure 10**). Creager (1999) found 2–4% anisotropy in the quasi-western hemisphere and only 0.5% in the quasi-eastern hemisphere. Other studies proposed an anisotropy level as high as 5% beneath the isotropic layer in the western hemisphere (Irving and Deuss, 2011b; Ouzounis and Creager, 2001). A mean value of 3% is generally accepted for the western hemisphere and 0.5–1% for the Eastern one.

The hemispherical pattern could partly be an artifact of the propagation through the lower mantle heterogeneities (Ishii et al., 2002a), but these heterogeneities fail to fully explain the observed pattern (Romanowicz et al., 2003). The South Sandwich Island events bias the polar path observations (Garcia et al., 2006; Tkalčić et al., 2002). Nevertheless, the hemispherical pattern in anisotropy seems to be a robust feature, and it is observed on both equatorial and polar data with opposite variations, as expected from relation [1] (Creager, 2000; Souriau et al., 2003a; Tanaka and Hamaguchi, 1997). In both hemispheres, the anisotropy is parallel to ERA. The isotropic velocity is nearly the same (Creager, 2000), which rules out an interpretation in terms of the difference in composition or fluid content. A variation in crystal alignment may explain the observations (Creager, 1999; Garcia, 2002b; Sun and Song, 2008). An alternative explanation invokes the difference in the thickness of the isotropic layer beneath the two hemispheres, which affects differently the PKP(DF) travel times so that it mimics variations in anisotropy (**Figure 10(c)**).

1.23.7.2.2.3 The innermost inner core

The presence of a different anisotropy in the central part of the core has been proposed to explain the travel time anomalies of PKP(DF) with nearly antipodal paths (Ishii and Dziewonski, 2002; Su and Dziewonski, 1995; **Figure 11**). A slow direction of propagation at about 45–55° from ERA is observed in the data sampling the innermost inner core (Calvet et al., 2006; Cao and Romanowicz, 2007; Ishii and Dziewonski, 2002, 2003; Niu and Chen, 2008; Sun and Song, 2008). Several studies have attempted to specify the anisotropy in this innermost inner core, with assumptions of transverse isotropy and symmetry axis parallel to ERA, but very different models have been obtained. Some models propose a fast axis parallel to ERA (Ishii and Dziewonski, 2003; Sun and Song, 2008) with a 3.5–3.7% anisotropy, higher than in the surrounding structures (**Figure 11(c)**, left). From a normal mode analysis, Beghein and Trampert (2003) propose a smooth model that favors a change in the sign of P-wave anisotropy in the central part of the inner core, thus an innermost inner core with a slow axis parallel to ERA (**Figure 11(c)**, right). An innermost inner core

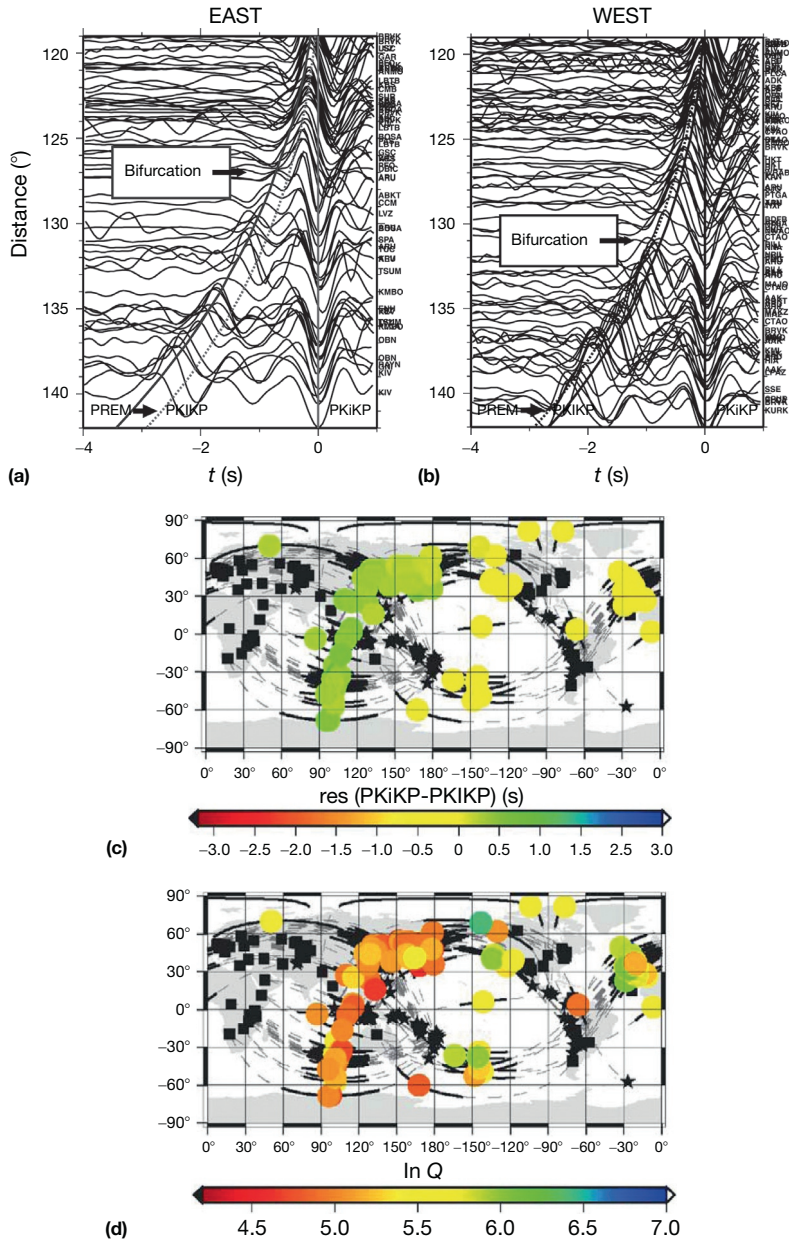

Figure 9 (a and b) Evidence for a hemispherical pattern in the uppermost inner core. Records of PKiKP and PKIKP phases sampling, respectively, the inner core boundary and the uppermost inner core beneath eastern and western hemispheres. The records are aligned on PKiKP, and the thick lines follow the phase maxima. Dashed line is the prediction for PREM. 'Bifurcation' corresponds to the separation of the two interfering phases. Note the difference between the two hemispheres for both differential travel times and PKIKP amplitudes, indicating a hemispherical heterogeneity in P-velocity and attenuation (reproduced from Wen L and Niu F (2002) Seismic velocity and attenuation structures in the top of the Earth's inner core. *Journal of Geophysical Research* 107 (B11): 2273). (c and d) Differential travel time residuals of PKiKP–PKIKP (in s) and quality factor (plotted in logarithmic scale) at the top of the inner core (depth 32–85 km below ICB, corresponding to distance 135–142°), showing that the eastern hemisphere is faster and more attenuating that the western hemisphere (reproduced from Cao A and Romanowicz B (2004) Hemispherical transition of seismic attenuation at the top of the earth's inner core. *Earth and Planetary Science Letters* 228: 243–253).

with P-wave anisotropy rate $\varepsilon = 0$ is obtained by Ishii et al. (2002a) (**Figure 11(c)**, middle). It turns out that, with the presently available data, the exact nature of the anisotropy in the innermost inner core is still hard to resolve and that the three families of models may be derived from the same PKP data, depending on data processing and assumptions used (Calvet et al., 2006). There is however some agreement about the mean radius of the innermost inner core, in the range 300–600 km for the most recent studies (Beghein and Trampert, 2003; Calvet et al., 2006; Cao and Romanowicz, 2007; Cormier and Li, 2002; Sun and Song, 2008). A sharp discontinuity at the top of the innermost inner core could not be detected (Cormier and Stroujkova, 2005; Garcia et al., 2006; Leyton et al., 2005; Niu and Chen, 2008). Cormier and

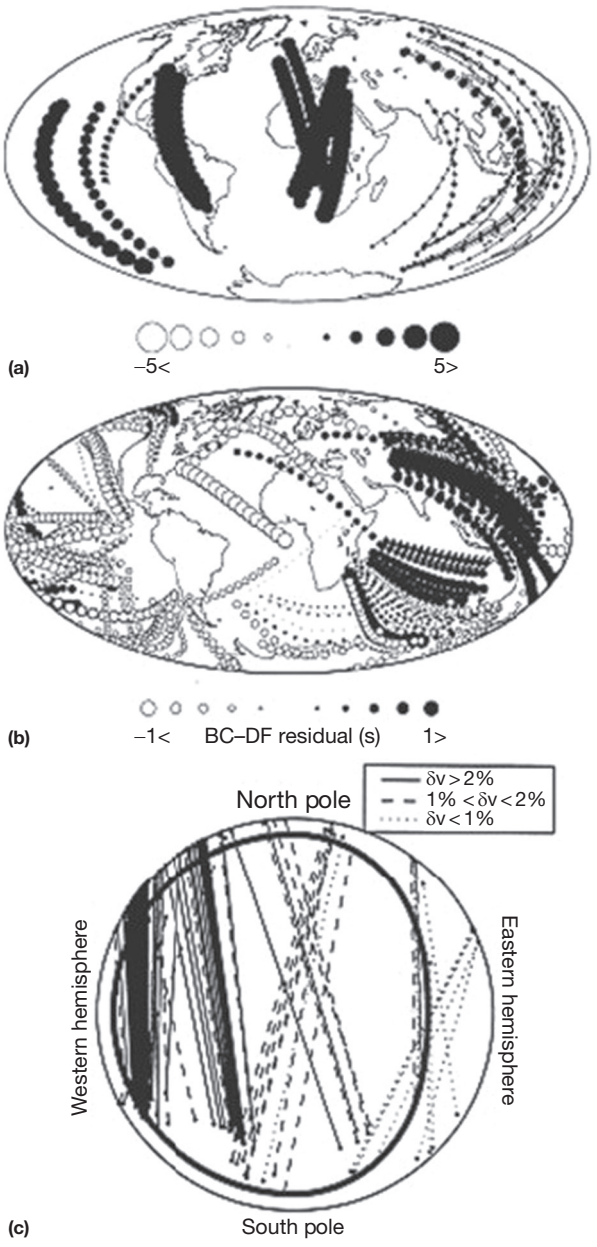

Figure 10 Evidence of a hemispherical pattern in the upper half of the inner core, as seen by PKP(BC)–PKP(DF) differential travel times. (a) Polar paths, the western hemisphere is faster than the eastern hemisphere; (b) the opposite is observed for East–West paths, but note the different scale (±5 s for (a), ±1 s for (b)) (reproduced from Tanaka S and Hamaguchi H (1997) Degree one heterogeneity and hemispherical variation of anisotropy in the inner core from PKP(BC)-PKP(DF) times. *Journal of Geophysical Research* 102: 2925–2938). (c) Interpretative cross section through the inner core looking from meridian 0°, showing the paths with their velocity anomalies, and a heavy line separating the isotropic asymmetric upper layer from the anisotropic structure (reproduced from Creager KC (2000) Inner core anisotropy and rotation. In: Dehant V, et al. (eds.) *Core Dynamics, Structure and Rotation*. *American Geodynamic Series*, vol. 31, pp. 89–114. Washington, DC: American Geophysical Union).

Stroujkova (2005) suggest the existence, between the two structures, of a broad, 50–100 km thick, transition zone at radius $r \sim 500$ km, which also coincides with a transition from low attenuation ($r < 500$ km) to high attenuation ($r > 500$ km) (Li and Cormier, 2002).

1.23.7.2.3 The origin of anisotropy

Seismic anisotropy in the inner core may be due to the preferred orientation of either anisotropic iron crystals, or elongated grains (each grain being an assemblage of crystals with similar orientations), or nonspherical fluid inclusions. In the first case, the seismic properties strongly depend on the elastic properties of the iron crystals and on their degree of alignment. In the second case, additional parameters are the orientation of crystals in each grain and the distribution of grain orientations in the medium. In the third case, the shape of inclusions and melt fraction are the key parameters.

The nature of iron or iron alloy at inner core conditions is a highly debated question. Details and references may be found in **Chapter 2.06**. The hexagonal closed-packed (hcp) structure of pure iron may be stable, but, because of the uncertainty on the temperature in the inner core, body-centered cubic (bcc), double hcp, and orthorhombic structures have also been proposed, on the basis of high-pressure experiments or theoretical computations. The presence of nickel or of light elements may stabilize the bcc or face-centered cubic phases. There is also no consensus on the elastic properties of the stable iron alloys and on the deformation slip system (Poirier and Price, 1999). Theoretical and experimental investigations on hcp iron have led to contradictory conclusions concerning the sign of P-wave anisotropy (fast or slow c-axis) depending on impurities and temperature, with even the possibility of a very low anisotropic rate. Iron in the bcc form, which is strongly anisotropic, provides an interesting alternative to hcp for explaining inner core anisotropy.

A degree of crystal alignment from 20% to 100% is necessary to explain the observed seismic anisotropy, depending on the elastic properties of the iron crystal. The distinct anisotropy in the innermost inner core suggests either the presence of a different iron phase (Kuwayama et al., 2008), or a different iron alloy, or some variation in the degree of crystal alignment. The reverse of the sign of the anisotropy at depth proposed by some seismic models may be explained by a variation with depth of the preferred orientation of a same form of iron.

A preferred orientation of ellipsoidal fluid inclusions is another possible mechanism to generate anisotropy (Singh et al., 2000). The presence of molten iron inclusions trapped in the iron lattice, at least in the upper half of the inner core, is proposed in support of the low S-velocity and high attenuation observed in that part of the inner core. The complex phase diagrams of iron alloys also favor a transition from solid to liquid with partial melting. A fluid volume fraction of 3–10%, present as oblate inclusions aligned in the equatorial plane, may explain the observed velocity anisotropy. However, as will be seen later, it fails to explain some characteristics of attenuation.

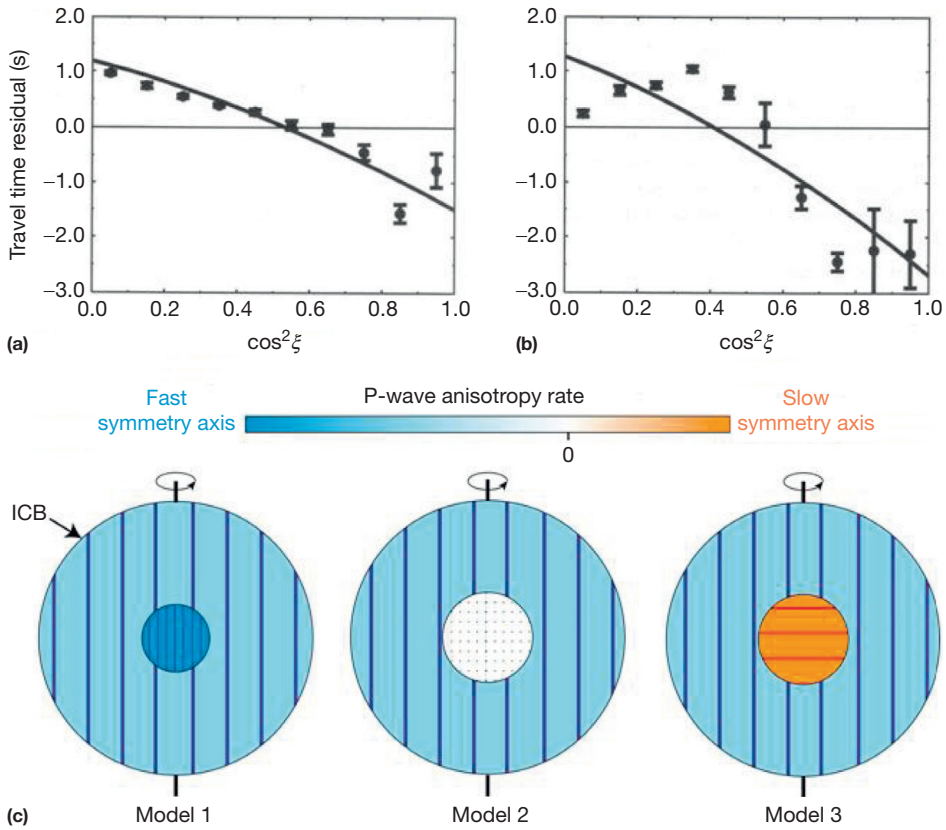

Figure 11 Evidence for a distinct anisotropy in the central part of the inner core. PKP(DF) residuals with respect to the reference model PREM, as a function of $\cos^2\xi$, where ξ is the ray angle with respect to the Earth's rotation axis inside the inner core (polar paths correspond to $\cos^2\xi = 1$). (a) Distance 153–155° (depth ~300 km beneath inner core boundary). (b) Distance 173–180° (turning point near the Earth's center). Black dots are the means of the observations with their error bars; thick lines are predictions for a uniform anisotropy model. Note on (b) the difference with the predictions for $\cos^2\xi \sim 0.35$ ($\xi \sim 55°$) ((a and b) reproduced from Ishii M and Dziewonski AM (2002) The innermost inner core of the Earth: Evidence for a change in anisotropic behaviour at the radius of about 300 km. *PNAS* 99: 14026–14030). (c) Cartoon showing the inner core with three possible innermost inner core structures that fit the data, with different P-wave anisotropy ((c) modified from Calvet M, Chevrot S, and Souriau A (2006) P-wave propagation in transversely isotropic media. II. Application to inner core anisotropy: Effects of data merging, parametrization and a priori information. *Physics of the Earth and Planetary Interiors* 156: 21–40).

The mechanism at the origin of a preferred alignment is also debated (see **Chapter 8.12** and Deguen, 2012, for reviews). The preferred orientation may be either acquired during the inner core growth (solidification texturing) or induced by deformation within the inner core. With solidification texturing, the internal structure is a record of inner core history since its formation, unless it has been erased by later processes. Solidification texturing may result from the growth of dendrites in the direction of heat extraction, thus in the radial direction with a cylindrical symmetry consistent with the convective pattern in the outer core (Bergman, 1997). Other texturing mechanisms able to generate anisotropy have been proposed, in particular alignment of iron crystal with the magnetic field (Karato, 1993) or compaction in the mushy zone at the ICB during inner core growth (Sumita et al., 1996).

Anisotropy may also result from inner core deformation. For example, it has been proposed that, because of the cylindrical pattern of the outer core flow that governs heat extraction, the inner core is expected to grow faster at the equator than near the poles. The adjustment of the inner core to its equilibrium figure is performed by a flow from the equator to poles (Yoshida et al., 1996), but the resulting deformation may be too weak to generate a substantial preferential orientation (Deguen, 2012). However, if the inner core has a compositional density stratification, the flow will be mostly concentrated in the upper layers, so that the central part of the core may keep the fossil texture of the primitive inner core (Deguen and Cardin, 2009).

Plastic deformation induced by convection inside the inner core may also produce anisotropy (Buffett, 2009; Cottaar and Buffett, 2012; Deguen and Cardin, 2011; Jeanloz and Wenk, 1988; Romanowicz et al., 1996; Weber and Machetel, 1992; Wenk et al., 2000). Convection may be driven by thermal or compositional instability in the inner core (Gubbins et al., 2013). The conditions required for triggering thermal convection are however not necessarily fulfilled, as they depend on debated parameters such as the thermal conductivity of iron, the amount of radioactive elements in the inner core, the conductivity profile of the outer core, and the heat flux at CMB (Buffett,

2000; Deguen, 2012; Hirose et al., 2013; Yukutake, 1998; see **Chapter 8.12**). Moreover, thermal convection hardly generates large-scale anisotropy, unless it is coupled with magnetic field (Buffett and Wenk, 2004; Karato, 1999).

1.23.7.3 Lateral Heterogeneities Inside the Inner Core and Scatterers

Lateral heterogeneities in the inner core may be due either to a change in isotropic velocity or to a change in anisotropy. In the first case (change in isotropic velocity), heterogeneities of thermal origin are ruled out, as the temperature is nearly uniform inside the inner core (Weber and Machetel, 1992). One may thus invoke either a chemical heterogeneity, a phase change, a change in the amount of partial melting, or a change in grain size of randomly oriented anisotropic grains. In the second case (change in anisotropy), the heterogeneity could be either an anisotropic domain with similar elastic properties but with different orientation or a domain with different anisotropic properties. Because of the poor geographic sampling, it is generally impossible to discriminate between bulk heterogeneities and anisotropy perturbations.

We have previously mentioned the existence of a hemispherical heterogeneity in isotropic velocity in the uppermost 85 km and a hemispherical variation in anisotropy in the depth range 100–700 km beneath ICB. We will later discuss the interpretation of this observation.

In the wavelength range 20–200 km, many studies have reported the possible existence of heterogeneities (Bréger et al., 1999; Collier and Helffrich, 2001; Creager, 1997; Kaneshima, 1996; Lindner et al., 2010; Song, 2000; Zhang et al., 2005). However, in none of these cases, it is possible to completely discard a mantle origin. A stochastic analysis of PKP(DF) at different distances shows that the heterogeneity in isotropic velocity does not exceed 0.3% for wavelengths 100–400 km (Garcia and Souriau, 2000b).

The existence of small-scale heterogeneities inside the uppermost inner core has been inferred from the observation of scattered energy in the coda of the PKiKP wave (Vidale and Earle, 2000). These scatterers raise great interest, because they may give information on the fine structure of the uppermost inner core, in particular on its possible dendritic growths and on the fate of grains and fluid inclusions with depth. They also contribute to the strong wave attenuation inside the inner core. The analysis of the PKiKP coda generally requires records from small aperture arrays (**Figure 12(a)**), in order to eliminate coda signal generated in the mantle or at the CMB. It is best observed in the frequency range 4–6 Hz (Koper et al., 2004; Poupinet and Kennett, 2004).

Two types of coda have been observed. In the first case, the signal may arrive emergently (**Figure 12(b)** and **12(c)**) with a spindle-shaped envelope lasting about 200 s after the theoretical arrival time of PKiKP, even if this phase is not observed (this is the case at distance ~70° because the reflection coefficient at the ICB is close to 0). This signal requires heterogeneities located in the uppermost 350 km of the inner core, with a size of the order of 1–10 km, and velocity contrast of 1–10%, or possibly more (Leyton and Koper, 2007a; Peng et al., 2008; Vidale and Earle, 2000). In the second case, the coda maximum is immediately after the PKiKP onset, with a rapid amplitude drop in the first seconds or tens of seconds, followed by a constant coda level during about 100–200 s (**Figure 12(d)**; Koper et al., 2004; Leyton and Koper, 2007b; Peng et al., 2008; Poupinet and Kennett, 2004; Vidale and Earle, 2000). Codas with sharp onsets may be better explained by scatterers at the ICB rather than in the inner core volume (Poupinet and Kennett, 2004; see **Chapter 1.24**).

Although the Earth sampling remains poor due to the limited number of small aperture arrays, the scatterer distribution appears uneven. The regions generating clear PKiKP coda are mostly beneath northern Pacific and eastern Asia, and the absence of coda is preferably observed beneath the Atlantic Ocean (Leyton and Koper, 2007b). This distribution may be related to the hemispherical pattern observed in the isotropic layer, even though additional observations are still necessary.

1.23.8 The Inner Core: Seismic Attenuation

The attenuation of seismic waves may give information on the physical nature of the inner core and on its texturing. In particular, if partial melting is present, a strong anelastic attenuation correlated with low S-velocities and low viscosity is expected. Energy loss may also be due to scattering induced by texture (anisotropic crystals with various orientations or shapes), by the presence of fluid pockets, or less likely by compositional heterogeneities. These two mechanisms induce wave dispersion thus PKP(DF) pulse broadening, but this effect is much more important for viscoelastic attenuation with flat relaxation spectrum than for forward scattering. The attenuation is usually quantified through the quality factor Q (attenuation is proportional to Q^{-1}). The total attenuation is expressed as the sum of anelastic (or intrinsic) attenuation Q_i^{-1} and scattering attenuation Q_s^{-1}:

$$Q^{-1} = Q_i^{-1} + Q_s^{-1} \quad [3]$$

(Sato et al., 2012).

P-wave attenuation Q_α^{-1} at high frequency is constrained by body waves, mostly by the amplitude of PKP(DF). For its anelastic contribution, Q_α depends on both the attenuation in bulk (Q_κ^{-1}) and in shear (Q_μ^{-1}), such as

$$Q_\alpha^{-1} = kQ_\mu^{-1} + (1-k)Q_\kappa^{-1} \quad [4]$$

where $k = 4/3 \times (v_S/v_P)^2$, v_P and v_S being the P- and S-velocities (see **Chapter 1.25**). Attenuation is also constrained by the normal modes, whose damping gives attenuation in the low-frequency part of the spectrum. Modes are mostly sensitive to the attenuation in shear and are insensitive to scattering by small-scale heterogeneities (<100 km). As for elastic parameters, they have a poor sensitivity to the central part of the core. A first difficulty in the interpretation of Q will thus result from the difference in the parameters and frequency bands sampled by body waves and normal modes. Another difficulty is to decipher the relative contributions of viscoelasticity and scattering.

1.23.8.1 P-Wave Attenuation: Depth Dependence and Hemispherical Variations

A comparison of the amplitude of PKP(DF) with the one of a nearby reference phase is often used to estimate the attenuation along the ray, using geometries that minimize source and mantle path contributions and assuming that Q is infinite in the liquid core. In the same way as for velocity models, the reference phase

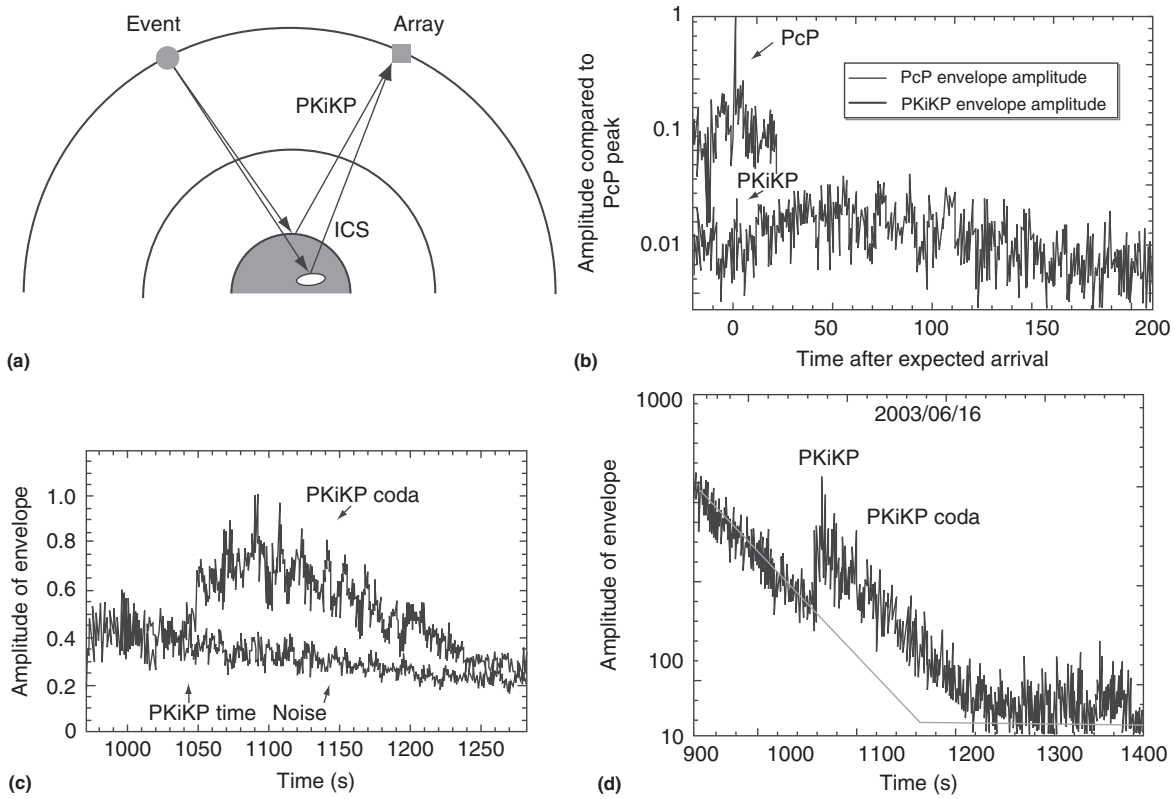

Figure 12 Detection of scatterers inside the inner core, from the coda of the PKiKP wave reflected at inner core boundary. (a) Principle of the method: energy arrival following PKiKP is detected at an array. (b) Comparison of the envelopes of the signal for the PcP wave reflected at core–mantle boundary and for the PKiKP wave, showing that the coda originates in the inner core, not in the mantle; the signals are stacks of two Novaya Zemlya nuclear tests. (c) Average of different PKiKP stacks for events at distances 60–70° from LASA in Montana, United States, compared to the noise ((a–c) reproduced from Vidale JE and Earle PS (2000) Fine-scale heterogeneity in the Earth's inner core. *Nature* 404: 273–275). (d) Same as (c) for an event at 74° from WRA array in Australia, showing a PKiKP coda with a different shape, an indication of variations in the scatterer properties inside the inner core ((d) reproduced from Poupinet G and Kennett BLN (2004) On the observation of high frequency PKiKP and its coda in Australia. *Physics of the Earth and Planetary Interiors* 146: 497–511).

is PKiKP in the uppermost 100 km and PKP(BC) for depths 100–300 km below the ICB with an extension down to 600 km using PKP(C_{diff}), but in this case, the amplitude of the reference phase becomes highly sensitive to the velocity gradient at the base of the liquid core. PKP(AB) is also sometimes used. The comparison of the two phases i and j is made either in the temporal domain, where the amplitude ratio A_i/A_j is measured on filtered traces, or in the spectral domain, taking advantage of the linearity of $\mathrm{Ln}(A_i/A_j)$ with frequency, if anelastic attenuation is dominant and not frequency-dependent. The intrinsic attenuation as a function of depth is then retrieved from the A_i/A_j ratio at different distances. A better approach uses waveform modeling, based on the comparison of the observed waveforms with the predictions of synthetic seismograms. It allows to sample any depth in the inner core, but it requires the knowledge of source and mantle structure (Li and Cormier, 2002; Tanaka, 2012).

The various studies come to a general agreement about a low Q_α in the uppermost inner core at frequency $f \sim 1$ Hz, with values ranging from 100 to 400 in the uppermost 200 km, increasing with depth up to 400–600 at 400 km beneath ICB (Bhattacharyya et al., 1993; Bolt, 1977; Cormier, 1981; Doornbos, 1974, 1983; Iritani et al., 2010; Ivan and Moloto-A-Kenguemba, 2007; Kazama et al., 2008; Niazi and Johnson, 1992; Ohtaki et al., 2012; Oreshin and Vinnik, 2004; Souriau and Roudil, 1995; Tanaka, 2012; Tseng et al., 2001; Yu and Wen, 2006a). These studies, which concern different regions, exhibit very different Q-profiles with depth. However, the error bars are large, and short wavelengths in mantle heterogeneities and CMB topography may strongly affect wave amplitudes (Bowers et al., 2000; Leyton and Koper, 2007a), which makes difficult the detection of regional variations, if any.

In the uppermost 50–100 km, a hemispherical pattern similar to the one observed for seismic velocities is clearly observed, the attenuation being stronger in the quasi-eastern hemisphere (40°–180° E) than in the quasi-western hemisphere (**Figure 9 (d)**). Q_α-values in the ranges 50–250 and 330–600 are reported for the eastern and western hemispheres, respectively (Cao and Romanowicz, 2004b; Garcia, 2002a; Monnereau et al., 2010; Tanaka, 2012; Wen and Niu, 2002; Yu and Wen, 2006a). Thus, high attenuation correlates with high velocity in the quasi-eastern hemisphere and low attenuation with low velocity in the quasi-western hemisphere. This correlation is opposite to that observed in the mantle, where it is ascribed to thermal effects. It is clearly detected down to 100 km but may be present deeper (Tanaka, 2012).

In the lowermost 500 km, waveform modeling of PKP at nearly antipodal distances reveals a Q-increase, together with a decrease in the scatter of the Q-values (Li and Cormier, 2002).

This central, high-Q zone approximately corresponds to the innermost inner core (**Figure 13**) and could correspond to a different fabric (Cormier and Stroujkova, 2005).

Studies based on spectral ratio analyses fail to detect a frequency dependence of Q_α in the narrow frequency range (0.2–2 Hz) sampled by body waves (e.g., Cormier, 1981; Souriau and Roudil, 1995), but waveform modeling, which takes into account the dispersive effect of viscoelasticity, suggests that such a frequency dependence is present (Cummins and Johnson, 1988b; Doornbos, 1983; Li and Cormier, 2002).

1.23.8.2 The Attenuation in Shear

The very strong attenuation in shear ($Q_\mu = 85$ in the PREM model) is mostly derived from the inversion of normal modes. Some specific studies of inner core-sensitive modes have proposed much larger Q-values, between 1500 and 4000 (Masters and Gilbert, 1981; Suda and Fukao, 1990), indicating that Q_μ must be high, about 3500. However, Widmer et al. (1991) have shown that these high Q_μ-values are possibly due to a misidentification of neighboring modes; they obtain $Q_\mu \sim 110$ for PKIKP-equivalent modes. On the other hand, Andrews et al. (2006) show that the Q-values may be affected by mode coupling and that Q_μ is low, so that the discrepancy between normal modes and body waves is small.

From waveform modeling of PKJKP, Cao and Romanowicz (2009) obtained a Q_μ-value of 315 ± 150. This is larger than the values given in PREM. As PKJKP better samples the Earth's center than modes, this discrepancy suggests that Q_μ increases with depth, as do Q_α and v_S.

The compatibility of modes and body waves has long been a subject of debate (see discussion in Romanowicz and Durek, 2000), because of the high Q_μ-values first proposed for inner core-sensitive modes. This seems no longer the case. However, the values of Q_α and Q_μ are not constrained well enough to infer the Q_κ value from relation [4], in particular to see if $Q_\kappa \gg Q_\mu$ as in the mantle. From the seismological results, it is also not possible to specify if several absorption bands are present in the inner core and what are the respective contributions of scattering and anelasticity.

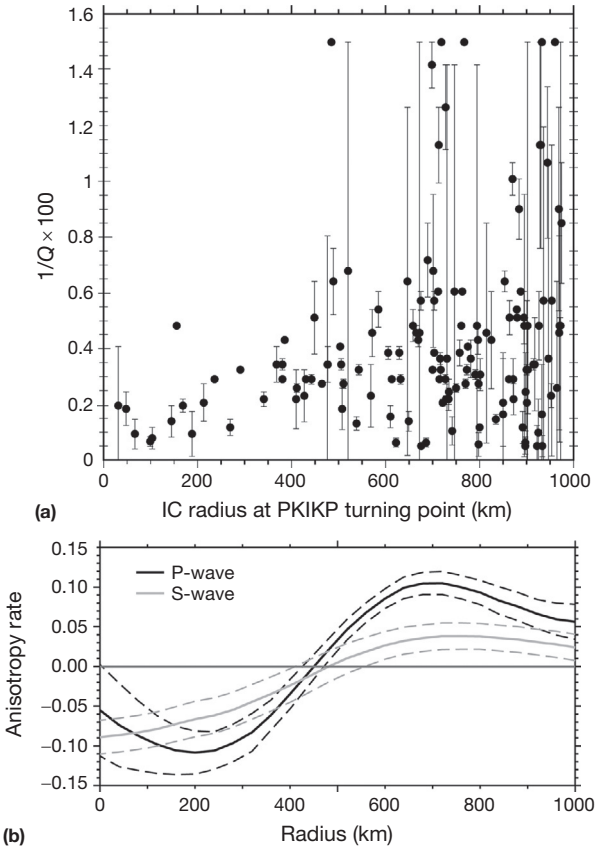

Figure 13 (a) Attenuation $1/Q_\alpha$ for PKP(DF) paths turning at different depths inside the inner core (Q_α is the P-wave quality factor) (reproduced from Cormier VF and Stroujkova A (2005) Waveform search for the innermost inner core. *Earth and Planetary Science Letters* 236: 96–105). (b) Two coefficients describing the anisotropy of P-wave velocity (black) and S-wave velocity (gray). Note the decrease of the attenuation and its smaller scatter inside the innermost inner core, where a different anisotropy is also observed (modified from Beghein C and Trampert J (2003) Robust normal mode constraints on inner core anisotropy from model space search. *Science* 299: 552–555).

1.23.8.3 The Anisotropy in Attenuation

A first direct evidence of anisotropy in P-wave attenuation is given by an analysis of PKP(DF) waves with turning points beneath the same region (Africa), but with various orientations with respect to ERA. Polar paths, which correspond to a faster propagation, also correspond to a stronger attenuation (Souriau and Romanowicz, 1996a; **Figure 14**). This result has been extended to the worldwide scale (Souriau and Romanowicz, 1996b) and to greater depth from waveform modeling of PKP at large distance (Cormier et al., 1998). Oreshin and Vinnik (2004) and Yu and Wen (2006b) confirm the dependence of attenuation with the ray angle with respect to ERA but show that it is observed in the western hemisphere only, where anisotropy in seismic velocity is the strongest one. Ray orientation also has an influence on the frequency dependence of attenuation and on dispersion (Souriau, 2009): For polar paths, the PKP(DF) wave is clearly dispersed and its amplitude decay is larger at high frequency than at low frequency, a frequency dependence that is not observed for equatorial paths.

From inner core-sensitive modes, Mäkinen and Deuss (2013) have identified a zonal pattern in anelasticity, suggesting that a cylindrical anisotropy in attenuation may also be present in shear, with again the high S-attenuation correlated to the high velocity.

1.23.8.4 Interpretation of Inner Core Attenuation

Two main mechanisms may contribute to attenuation: viscoelasticity (Cormier, 1981; Doornbos, 1974; Li and Cormier, 2002) and scattering (Calvet and Margerin, 2008; Cormier, 2007; Cormier and Li, 2002). They may be present simultaneously in the inner core.

A viscoelastic model with frequency-dependent attenuation is able to explain the main characteristics of attenuation in the body-wave domain (Li and Cormier, 2002), but the low dispersion of the data requires very particular conditions to be explained with this mechanism. Viscoelasticity could be

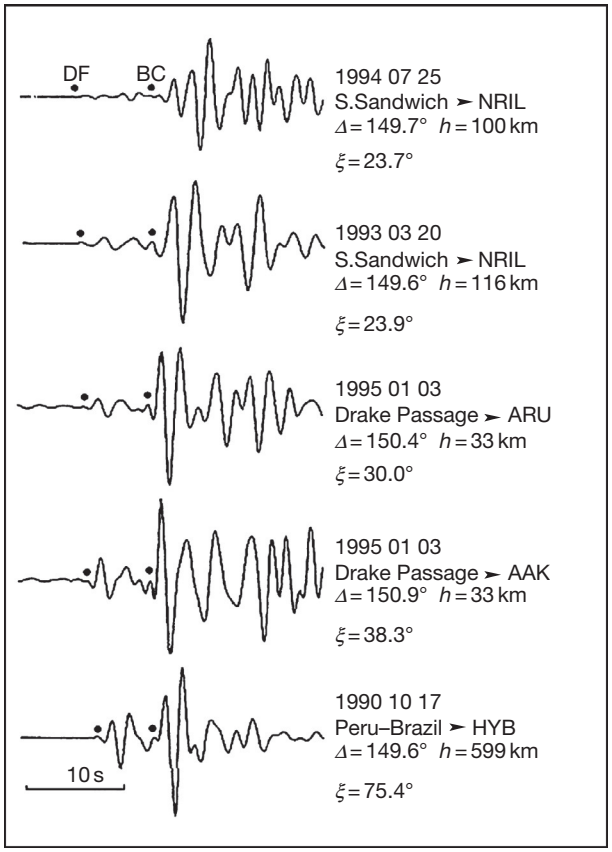

Figure 14 Evidence for anisotropy in attenuation correlated to the anisotropy in velocity, from records corresponding to paths turning in the inner core beneath Africa, with nearly the same distance Δ, but with different orientations ξ with respect to the Earth's rotation axis (h is the focal depth). PKP(BC) being the reference phase, note the fast propagation (large BC−DF time) and strong attenuation (small DF/BC amplitude) for nearly polar paths (small ξ). Data are band-pass filtered at 2 s. Reproduced from Souriau A and Romanowicz B (1996) Anisotropy in inner core attenuation: A new type of data to constrain the nature of the solid core. *Geophysical Research Letters* 23: 1–4.

present at the top of the inner core, because of a possible high proportion of fluid inclusions trapped in the iron lattice (Fearn et al., 1981; Loper and Roberts, 1981). However, the correlation of high (respectively low) attenuation with high (respectively low) velocity observed in the uppermost isotropic layer is opposite to model predictions (O'Connell and Budianski, 1977), which indicates that this mechanism is not predominant. From PKiKP coda analysis, Leyton and Koper (2007b) obtained a coda Q-value close to 500 and inferred that scattering attenuation must be at least comparable, or possibly larger, than anelastic attenuation in the uppermost inner core.

The difficulties met with the anelastic model are overcome with a scattering model Cormier (2002). The observation of PKiKP coda is a strong argument in favor of this mechanism. Scattering attenuation depends on the typical scale length of the heterogeneities and on the amplitude of velocity perturbations. The PKP(DF) attenuation may be explained by a heterogeneous random medium with P-wave velocity perturbations of ~8% and typical scale lengths 0.5–2 km (Cormier et al., 1998) or slightly larger, about 10 km (Cormier and Li, 2002). From the energy envelopes of PKiKP coda waves, Vidale and Earle (2000) found heterogeneities of about 2 km with velocity fluctuations of only 1.2% in the uppermost 300 km of the inner core. Cormier (2007) proposed that these coda waves are induced by reverberation on a platelike fabric developing at ICB under the shearing of the tangential outer core flow and obtained perturbations of 10%. Calvet and Margerin (2008) developed a scattering model in which the heterogeneities result from the random orientation of grains with similar anisotropy. They showed that iron grains of size ~400 m may easily explain Q_α-values in the range 300–600. The hemispherical variations may be due either to a variation of the preferred orientation in the texture (Cormier, 2007) or to a grain size difference between the two hemispheres (Monnereau et al., 2010). We will return to this point in the next section. On the other hand, from laboratory crystallization experiments and from geodynamic considerations, Bergman (1997, 1998) found a grain width around 200 m, which is in rather good agreement with seismological estimates.

The anisotropy in attenuation is too large to be explained by wave-front distortion due to velocity anisotropy. The correlation between anisotropy in velocity and anisotropy in attenuation, with the high attenuation axis corresponding to the fast axis parallel to ERA and low attenuation corresponding to slow propagation parallel to the equatorial plane, may give some indications about the mechanisms at the origin of anisotropy. If the velocity anisotropy were due to fluid inclusions, as proposed by Singh et al. (2000), the opposite correlation would be observed (Peacock and Hudson, 1990). The right correlation may be observed in anelastic anisotropic media characterized by complex stiffness tensor (Carcione and Cavallini, 1994). Again, scattering (by anisotropic crystals or elongated heterogeneities) appears to be the most plausible attenuation mechanism to explain the observed correlation for anisotropy. Following the dendritic model of Bergman (1997), Cormier (2007) proposed that radially oriented, elongated structures may explain both velocity and attenuation. The strong attenuation of paths parallel to ERA would be a consequence of the large number of grain boundaries crossed by the seismic rays.

Scattering is likely the predominant attenuation mechanism at high and intermediate frequencies (0.02–2 Hz) (Cormier and Li, 2002), but not in the normal mode frequency band (0.001–0.01 Hz) where viscoelasticity is favored. When scatterers cannot been directly detected from coda waves, deciphering the relative contributions of viscoelasticity and scattering relies on measurements of induced effects, such as pulse distortion or wave dispersion, which are difficult to observe (Cormier and Li, 2002; Li and Cormier, 2002).

1.23.8.5 Origin of the Hemispherical Pattern in the Uppermost Inner Core

The hemispherical pattern is certainly the most intriguing feature of the inner core. It appears at two levels: (1) in the uppermost isotropic layer, where the quasi-eastern hemisphere has high velocity and high attenuation compared to the Western one, and (2) in the depth range 100–700 km below ICB, where the western hemisphere has strong anisotropy in both velocity and attenuation with the fast axis and high

attenuation axis parallel to ERA, compared to the eastern hemisphere where anisotropy is weak for both velocity and attenuation. There is to date no satisfying explanation of these different observations. Scattering related to the iron crystal structure and diffusion related to fluid inclusions have both been invoked to explain the uppermost inner core dichotomy. Also, several geodynamic models are possible; some of them invoke simultaneous freezing and melting at ICB.

Cao and Romanowicz (2004b) argue that hemispherical variations of heat flow near ICB may induce variations in the melt fraction content and/or connectivity of liquid inclusions in a mushy zone. The liquid inclusions may be well isolated in the eastern hemisphere, while they may remain partly connected in the western hemisphere that may be colder and freezing more rapidly (Cao and Romanowicz, 2004b). The effect of the connectivity of fluids on the seismic properties is however highly complex (O'Connell and Budianski, 1977).

From laboratory experiments, it is inferred that textures acquired by solidification at the ICB may be closely coupled to heat extraction by the fluid flow at the base of the outer core (Bergman et al., 2002). Cormier (2007) proposes that, in actively crystallizing regions associated to outer core upwellings, the fabric is characterized by dendrites elongated in the radial direction with hcp iron c-axis perpendicular to the dendrite elongation (Bergman et al., 2002). This texture results in high velocity, strong PKP(DF) attenuation, and weak PKiKP coda (**Figure 15(a)**) and may represent the eastern hemisphere structure. By contrast, when the outer core flow is tangent to ICB, the longer scale lengths of the texture tend to be parallel to ICB, and the PKIKP attenuation is less efficient. Such a texture may develop in the western hemisphere where anisotropy is also observed. Lateral variations from strong to weak velocity and attenuation and from weak to strongly backscattered PKiKP coda may thus be explained by a textural variation from vertical- to horizontal-oriented platelike structures (Cormier, 2007). However, Cormier et al. (2011) argue that the long PKiKP codas observed by Peng et al. (2008) in the western hemisphere are better explained with an isotropic distribution of scale lengths (**Figure 15(b)**), together with viscoelastic dissipation.

Thermal heterogeneities may drastically affect fluid flow in the outer core, which in turn induces textural heterogeneity in the inner core (Sumita and Olson, 1999). Following this idea, Aubert et al. (2008) developed a model of thermochemical convection in the outer core, in which long-term cyclonic circulation beneath Asia causes fast freezing in the eastern hemisphere and slow freezing in the Western one where well-textured crystals develop (**Figure 16(a)**). The hemispherical texture and thermal conditions are thus opposite to those of Cormier et al. (2011) and Cao and Romanowicz (2004b). On the other hand, from geodynamo simulations, Gubbins et al. (2011) propose that melting and freezing may occur simultaneously at different places at the ICB, a broad melting zone being related to an outer core upwelling beneath the Pacific in the western hemisphere.

Thermal convection inside the inner core has also been proposed to explain the East–West seismic dichotomy. Convection with open boundaries (thus the possibility of freezing or melting at ICB) may induce a solid translation of the inner core (Alboussière et al., 2010; Monnereau et al., 2010). For large viscosity, the main convective mode is a global translation of

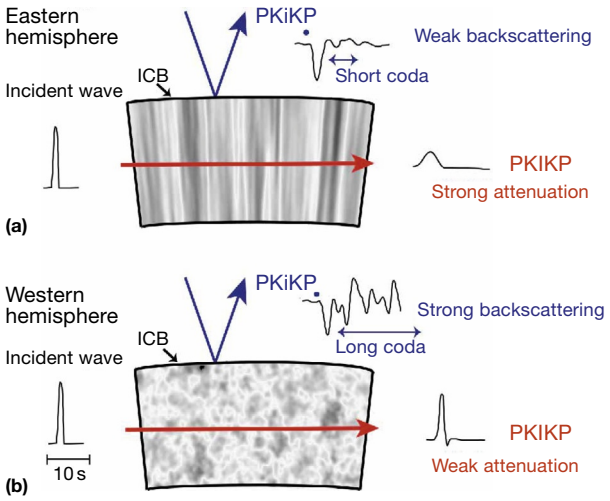

Figure 15 Possible textures explaining the hemispherical dichotomy in the uppermost inner core and their consequences for seismic waves. (a) Dendrites developing perpendicularly to inner core boundary (ICB), a possible model for the eastern hemisphere. The transmitted PKP(DF) wave (also noted PKIKP) is strongly dispersed and attenuated by the numerous boundaries encountered by the seismic ray (note the broadening of the signal), whereas the reflected PKiKP wave is almost undistorted. (b) Randomly distributed scatterers, a possible model for the western hemisphere. The strong backscattering is responsible for the long coda of transmitted waves. Modified from Cormier VF (2007) Texture of the uppermost inner core from forward- and backscattered seismic waves. *Earth and Planetary Science Letters* 258: 442–453.

the inner core with melting at the surface of one hemisphere and solidification at the other one (**Figure 16(b)**). Monnereau et al. (2010) suggest that grains grow during their transit from the crystallizing western hemisphere to the melting eastern hemisphere. Multiple scattering modeling of seismic waves in iron crystal aggregate explains the East–West dichotomy in both velocity and attenuation. The direction of translation and the resulting crystallizing hemisphere are however subjects of debate, as they depend on the forcing by thermal heterogeneities and on the liquid core flow; moreover, they may evolve with time (Aubert, 2013; Olson and Deguen, 2012).

The hemispherical pattern in anisotropy at depth is not fully explained by any models. For example, the translation mode does not produce any deformation. However, high-degree convective modes may develop for decreasing viscosity and induce texturing in the colder hemisphere (Mizzon and Monnereau, 2013). On the other hand, to explain the weak anisotropy in the eastern hemisphere, Bergman et al. (2010) suggest that the anisotropic solidification texture acquired in the western hemisphere is gradually lost during translation toward the melting side, as the result of thermal annealing.

1.23.9 Inner Core: Differential Rotation with Respect to the Mantle

A differential eastward rotation of the inner core with respect to the mantle (i.e., a faster rotation of the inner core) is predicted by some models of geodynamo (e.g., Aubert and Dumberry,

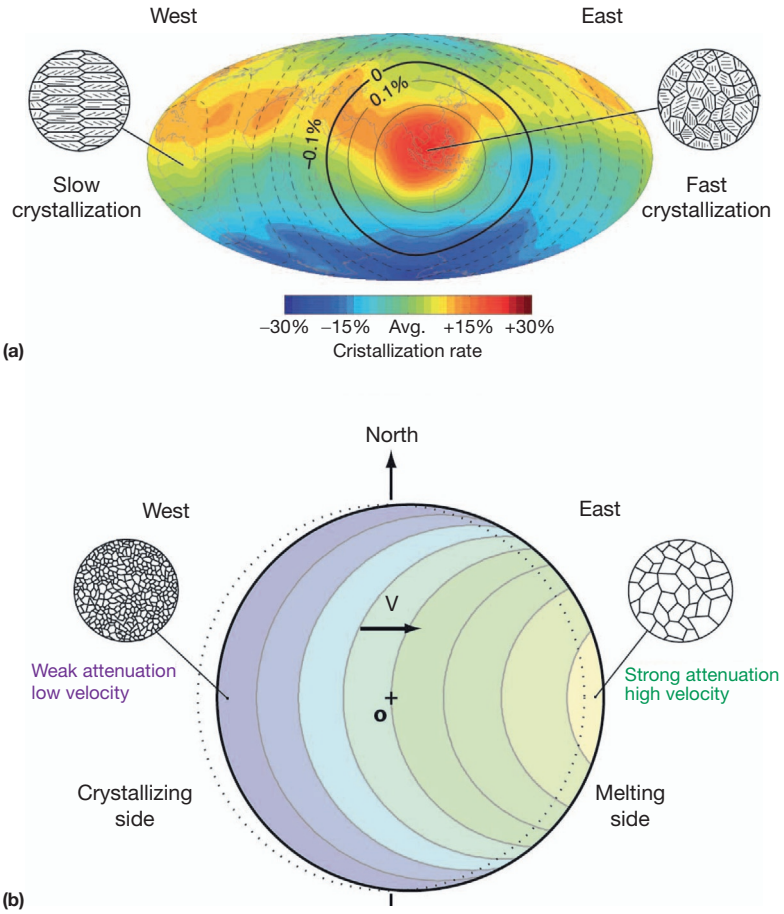

Figure 16 Cartoons illustrating two growth models at the origin of the seismic hemispherical pattern and possible resulting textures (grain size and orientation) in the uppermost inner core. (a) Relative crystallization rate (with respect to mean rate) at inner core surface resulting from heat extraction at ICB induced by the forcing of the thermal heterogeneities at CMB; superimposed is the seismic velocity degree one from Tanaka and Hamaguchi (1997) (modified from Aubert J, Amit H, Hulot G, and Olson P (2008) Thermochemical flows couple the Earth's inner core growth to mantle heterogeneity. *Nature* 454: 758–761). (b) Cross-section showing the age distribution in the inner core resulting from solid translation V (here from left to right, from dashed to plain positions). The age increases from the crystallizing side (blue) to the melting side (yellow) (reproduced from Monnereau M, Calvet M, Margerin L, and Souriau A (2010) Lopsided growth of Earth's inner core. *Science* 328: 1014–1017).

2011; Aurnou et al., 1996; Glatzmaier and Roberts, 1996; Gubbins, 1981; see Volume 8). The predicted rotation rate is as large as 2–3° year^{-1}; thus, time-dependent phenomenons induced by this rotation could possibly be detected by the propagation of seismic waves. At the same time, gravimetric coupling predicts that inner core heterogeneities and topography induced by mantle heterogeneities must be locked by the mantle gravity field, forcing the inner core to rotate at the same rate as the mantle (Buffett, 1997; see **Chapter 8.08**). Thus, the inner core rotation may give important constraints on the balance of these two antagonist effects and on their dynamic and structural consequences.

The basic idea for detecting inner core rotation is to track inner core heterogeneities during a long time, either along particular seismic paths that are unchanged during decades (**Figure 17(a)**) or at the worldwide scale. Seismological data are available since the 1950s, but high-quality digital data required for accurate analyses are available only since the 1980s. Before the 1970s, mechanical and optical limitations on recording systems made it hard to reach the accuracy level (< 0.1 s) required for such studies.

1.23.9.1 Tracking the Drift of a Heterogeneity Along a Stable Seismic Path

The heterogeneity could be either an identified small-scale heterogeneity inside the inner core (Creager, 1997; Lindner et al., 2010; Mäkinen and Deuss, 2011; Song, 2000), or the transition between the two inner core hemispheres (Souriau and Poupinet, 2003; Waszek et al., 2011), or scatterers (Vidale and Earle, 2005; Vidale et al., 2000), or the topography at ICB (Cao et al., 2007; Souriau, 1989; Wen, 2006).

Song and Richards (1996) proposed to use the apparent wobble of the tilted anisotropy symmetry axis, and, from the analysis of a 30-year data of South Sandwich Island events recorded at College Station (COL) in Alaska, they obtained a 1.1° year^{-1} eastward rotation rate. Soon after, another estimation at 3° year^{-1} was obtained from a worldwide analysis of

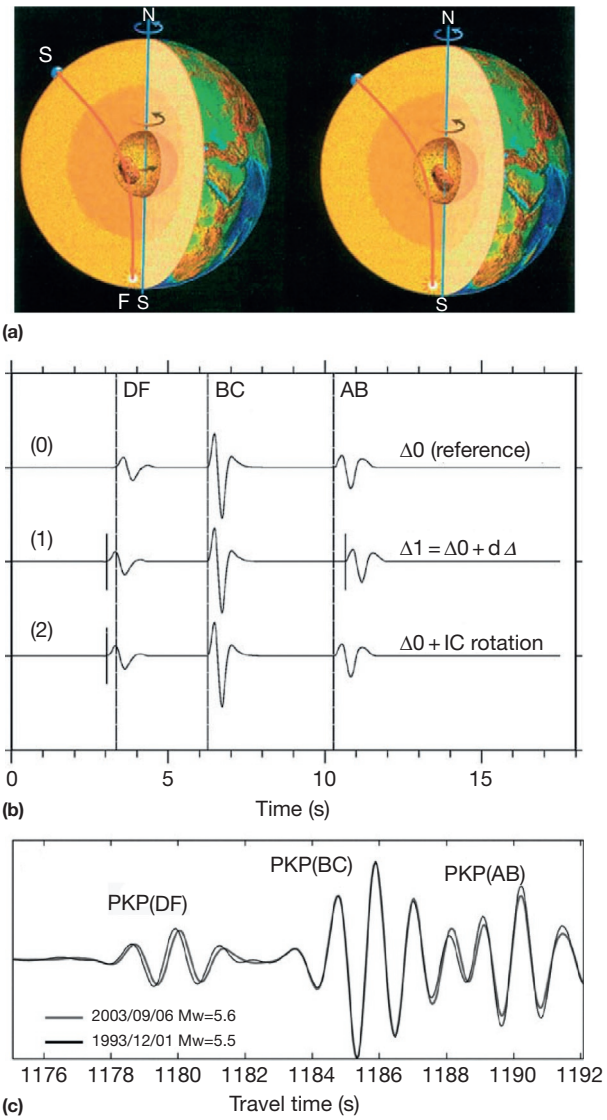

Figure 17 (a) Principle of the detection of an inner core differential rotation with respect to the mantle, from the drift of an inner core heterogeneity through a seismic ray. Figure on the right corresponds to a later stage than figure on the left, assuming an eastward (faster) rotation of the inner core. (b) Principle of doublets for discriminating between inner core rotation and earthquake mislocation, by the use of the three PKP phases (DF, BC, and AB). A small difference in location, giving a difference in epicentral distance $d\Delta$ with respect to the reference event at distance $\Delta 0$ (trace 0), results in a proportional variation of (BC−DF) and (AB−BC) (trace 1) compared to (0). Trace (2) corresponds to an event with same location as (0), but the DF time only is modified, due to the drift of an inner core heterogeneity along the DF ray ((b) reproduced from Souriau A, Garcia R, and Poupinet G (2003) The seismological picture of the inner core: Structure and rotation. *Compte-Rendus Geoscience* 335: 51–63). (c) Example of doublet of two South Sandwich Island events separated by 10 years (1993, 2003) recorded in Alaska. The DF time shift is interpreted as due to inner core rotation ((c) reproduced from Zhang J, Song X, Li Y, Richards PG, Sun X, and Waldhauser F (2005) Inner core differential motion confirmed by earthquake waveform doublets. *Science* 309: 1357–1360).

travel times (Su et al., 1996). These puzzling observations started an interesting debate that involved both observational and theoretical aspects, even though the interpretation in terms of tilt axis was criticized (Souriau et al., 1997). The data of South Sandwich Island events at COL were reinterpreted as due to the drift of a heterogeneity (Creager, 1997), leading to a rotation rate of 0–0.3° year^{-1}, depending on mantle heterogeneities. A difficulty arises from the perturbing signal of the subduction zones on both source and station sides. Paths that avoid subduction zones, for example, Novaya Zemlya nuclear tests recorded at Antarctic stations, led to time perturbations generally smaller than those observed for the path from South Sandwich Island to COL and sometimes of opposite sign (e.g., Isse and Nakanishi, 2002; Li and Richards, 2003b; Souriau, 1998). On the other hand, despite some attempts to retrieve simultaneously inner core structure and rotation, the existence of an inner core heterogeneity along the investigated path is generally difficult to assess (see Souriau and Poupinet, 2003; and Song, 2003, for reviews and discussions of the earlier results).

Another difficulty is to eliminate focal mislocations. Seismological networks have evolved with time, inducing systematic, time variable, location biases (Kennett and Engdahl, 1991) that could induce effects similar to those due to rotation. A way to circumvent this difficulty is to use doublets, that is, pairs of events with nearly the same focal location, recorded at the same station with similar waveforms (Poupinet et al., 1984). A difference in distance for the two events results in an apparent dilatation or contraction of one record with respect to the other (**Figure 17(b)**), whereas an inner core heterogeneity encountered along the path affects the PKP(DF) travel time only.

The doublet approach, first applied to the path from South Sandwich Island to COL (Poupinet et al., 2000), has been widely applied since. Despite the use of high-quality doublets, controversial results depending on the method refinement and on the paths considered have been obtained. In some cases, the same high-quality doublet (**Figure 17(c)**) recorded at different stations led to different interpretations involving either inner core rotation or variations in inner core radius (Cao et al., 2007; Wen, 2006; Zhang et al., 2005).

The results obtained along particular paths are globally inconsistent. Some of the paths give an eastward rotation, with rotation rates in the range 0.1–0.2° year^{-1} for most of them (Cao et al., 2007; Mäkinen and Deuss, 2011) and higher values (0.2 and 0.6° year^{-1}) for the paths from South Sandwich Island to Alaska (Lindner et al., 2010; Song, 2000; Tkalčić et al., 2013; Zhang et al., 2005). Some paths do not detect any variation (Collier and Helffrich, 2001; Isse and Nakanishi, 2002; Poupinet et al., 2000; Zhang et al., 2008) or a westward rotation (Mäkinen and Deuss, 2011). Nonmonotonic rotation (Lindner et al., 2010; Tkalčić et al., 2013) or inner core oscillations (Collier and Helffrich, 2001) have also been proposed. The incompatibility among the different paths led Mäkinen and Deuss (2011) to reject inner core rotation with rates exceeding 0.1° year^{-1}.

Scatterers inside the inner core may also be used. Their main advantage is the rapid modification of the diffraction

pattern when they move, thus the possibility to detect inner core rotation in a few years. Vidale et al. (2000) analyzed the scattered waves that follow PKiKP for two closely located Novaya Zemlya nuclear tests at 3-year interval and recorded at LASA (large aperture seismic array in Montana, United States). The change in the diffraction pattern may be explained by a $0.15^\circ\,\text{year}^{-1}$ faster rotation of the inner core. A similar analysis, carried out on seven Mururoa (Pacific Ocean) French nuclear tests recorded at NORSAR (Norway), gives a rotation rate of $0.05–0.10^\circ\,\text{year}^{-1}$ (Vidale and Earle, 2005). The location of the nuclear tests is however not known very accurately (within 5–10 km) so that systematic biases due to source location cannot be ruled out.

1.23.9.2 A Search for a Differential Rotation with a Worldwide Approach

Local or regional heterogeneities inside the inner core are difficult to identify; they may be hidden by mantle heterogeneities and are smeared by the PKP(DF) Fresnel zone. A way to avoid this problem is to solve inner core rotation at the worldwide scale.

Several studies are based on the data from the ISC catalog, using statistical approaches. The results are often poorly conclusive, either because of the uneven Earth sampling with time (Su et al., 1996) or because of the lack of resolution of the data (Souriau and Poupinet, 2003).

The most reliable results are obtained from the analysis of normal modes at two different epochs. They rely on the identification of long wavelength, even degree heterogeneities inside the inner core, after correction for mantle heterogeneities. Inner core heterogeneities are responsible for splitting of the resonance peaks, which are described by splitting functions whose time variations are analyzed. This method has the potential to estimate accurately the rotation rate, but a good Earth coverage and the use of a large number of modes are necessary. Sharrock and Woodhouse (1998) analyzed seven modes for the period 1977–96, and they obtained a westward rotation rate of $0.5–2.5^\circ\,\text{year}^{-1}$, depending on the mode considered. Laske and Masters (1999) analyzed a larger data set and found that the rotation rate is essentially zero over 20 years ($0 \pm 0.2^\circ\,\text{year}^{-1}$). A later study (Laske and Masters, 2003), with more modes and more events, shows that the results are consistent for different mantle corrections and again emphasizes the dependence of the result on the mode considered, with rotation rates either positive or negative (**Figure 18**). The mean eastward rotation rate is $0.13 \pm 0.11^\circ\,\text{year}^{-1}$, thus a rotation that is barely significant.

1.23.9.3 Rotation or No Rotation? Implications

After two decades of controversies, the absence of steady rotation now seems favored in the light of the most recent results, which show inconsistencies among the rotation rates obtained for different paths and for different normal modes. Note however that the resolution of the different methods hardly exceeds

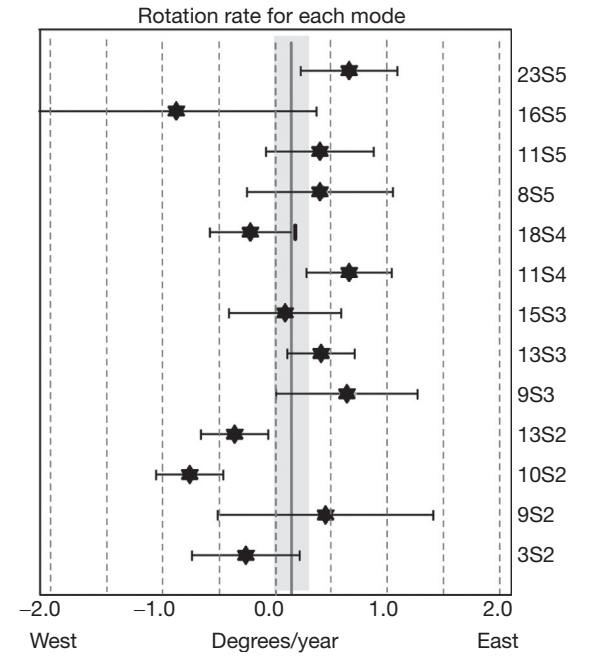

Figure 18 Inner core rotation rates obtained for various inner core-sensitive modes, after correction for mantle heterogeneities. The results vary with modes and are often compatible with a null rotation. Light gray area, least square fit of the rotation rate for all the modes. Modified from Laske G and Masters G (2003) The Earth's free oscillations and the differential rotation of the inner core. In: Dehant V, et al. (eds.) *Earth's Core, Dynamics, Structure, Rotation. Geodynamics Series*, vol. 31, pp. 5–22. Washington, DC: American Geophysical Union; Courtesy of G. Laske.

$0.05^\circ\,\text{year}^{-1}$, so that a rotation or oscillation rates lower than this value cannot be ruled out.

The largest rotation rates have been obtained for the paths from SSI to Alaska (time variations of $0.01\ \text{s year}^{-1}$ and rotation rates between 0.05 and $1.1^\circ\,\text{year}^{-1}$), which is the best sampled polar path. Unfortunately, it is also highly anomalous, as revealed by the large scatter of its PKP(DF) residuals (Bréger et al., 1999), and subject to criticism because of the difficulty to correct for mantle contributions and hypocentral mislocations. Moreover, PKP(DF) emerges barely from the noise, because of the strong attenuation in the polar direction (Li and Richards, 2003a). At the other end, the lower rotation rates are obtained from global studies, which are less dependent on the identification of a single heterogeneity. They are globally compatible with the absence of rotation. The analyses of reflected waves and scattered waves also lead to low rotation rates, $0.05–0.15^\circ\,\text{year}^{-1}$.

Whatever the path considered, and even for global Earth investigations, the main uncertainty concerns the heterogeneities that are used to quantify the differential rotation. The inner core sampling is generally too sparse to reliably map these heterogeneities. Only the quasi-hemispherical heterogeneity is robustly identified; temporal variations for this structure have been detected neither from body waves nor from normal modes (Souriau and Poupinet, 2003; Waszek et al., 2011).

The geodynamic consequences of an inner core rotation depend on the relative contributions of the gravitational, geomagnetic, and viscous couplings. These antagonistic effects may result in large ($\sim 0.1^\circ\,\text{year}^{-1}$) inner core oscillations with respect to the mantle about ERA, superimposed to a small steady rotation (Aubert and Dumberry, 2011; Buffett and Glatzmaier, 2000), but these results are strongly model-dependent. Some important parameters are the viscosity of the liquid core at the ICB and the viscosity of the inner core. The possible presence of a slurry layer above the ICB may contribute to increase the liquid core viscosity at the ICB. On the other hand, the inner core viscosity controls the ability of the inner core to deform in order to permanently adjust its shape to the mantle gravity field (Buffett, 1997).

If differential rotation is present, viscous deformation may concern the uppermost inner core only or the whole inner core, depending on the viscosity of the inner core. If the deformation is confined in an uppermost low viscosity layer, the strong shear induced by the viscous deformation would induce a preferred orientation of crystals or melt inclusions, in contradiction with the absence of anisotropy in the uppermost inner core. If the deformation involves the whole inner core, the inner core will be continuously mixed by the viscous flow, with relaxation times of the order of 3000 years. It will be hard in this context to maintain heterogeneities inside the inner core. Moreover, the readjustment flow will have a degree-two symmetry (Buffett, 1997); thus, it will induce a degree-four pattern in anisotropy, which is not observed. It is also difficult to reconcile a large rotation rate with the generation of a hemispherical pattern in the inner core, whose textural development requires a long-term coupling with the mantle, even though it is internally driven (see discussion in Deguen, 2012). A variation with depth of the hemispherical pattern, which could be a signature of the differential rotation during inner core growth (Waszek et al., 2011), may not easily be resolved with the seismological data because of the large Fresnel zone of the PKP waves. A large steady rotation thus seems unrealistic. This is consistent with dynamic models, which predict that the coupled effects of electromagnetic, viscous, and gravitational forces result in a mean rotation rate far below the detection threshold of seismological methods.

Inner core oscillations of the order of $0.1^\circ\,\text{year}^{-1}$ with typical period of 75 years are predicted from models taking into account the different torques acting on the inner core, although it must be noted that the fluctuations are far from being periodic (Aubert and Dumberry, 2011; Buffett and Glatzmaier, 2000). It has been suggested that the rotation observed in some studies could be part of an oscillation. This also seems unrealistic, because the different results relevant to a same time period do not give the same rotation rate (Mäkinen and Deuss, 2011).

The only way to reconcile the different observations is to imagine time-variable phenomena inside the inner core or at the ICB, which would have a local extension and which would be strong enough to give a seismological signature (Cao and Romanowicz, 2007; Mäkinen and Deuss, 2011; Sharrock and Woodhouse, 1998). It could be, for example, a modification in a slurry layer above ICB or in the mushy zone in the uppermost inner core. Alternatively, the source of variation could be outside the core. Finally, and more likely, the observations may still suffer from uncorrected mantle contributions and source location biases, even though doublet analyses remove most of them. In any case, more seismological and theoretical analyses are still necessary to make progress on this subject.

1.23.10 Conclusion

From the previous analyses, it may seem that the picture of the core is rather confused and that few characteristics meet a general agreement. This is true: the core is still a wide, almost virgin area of investigation compared to other structures in the Earth. Its deep location beneath heterogeneous layers (in particular D″ at the base of the mantle), together with the complexity of the physics of the core, let us anticipate that it will still long be a subject of controversy. At the same time, and for the same reasons, it is one of the most attractive objects for Earth scientists. We will attempt to summarize hereafter the seismological results that are considered as almost certain, those that are highly probable, and those that are still controversial or doubtful. We will then give some elements for future research.

1.23.10.1 Summary of the Results

The radii of the outer core and inner core are known with a good accuracy: 3480 ± 1 km for the CMB and 1215–1221 km for the ICB. These two boundaries are first-order discontinuities for the seismic waves (thickness < 2 km). The CMB has a small extra flattening (of < 500 m) with respect to its equilibrium figure and possibly a weak topography at different wavelengths, which may hardly exceed 4 km. The ICB has roughly the shape of its hydrostatic figure (thus is nearly spherical), with probably a long wavelength topography of no more than a few hundred meters, undetectable by seismology.

The liquid core is homogeneous from the seismological point of view, with neutral stratification except at the ICB, and perhaps at the CMB. Its density, well constrained by normal modes, shows a deficit with respect to molten iron that implies the presence of about 10% by weight of light elements. The base of the liquid core exhibits an ~ 150 km thick layer with low velocity gradient and increased density; it may correspond to an enrichment in iron. A repeated freezing and melting at the ICB is a possible mechanism to generate this layer. The liquid core has everywhere a nearly infinite quality factor. It is thus a transparent medium for seismic waves. It has a zero rigidity and a low viscosity; thus, it cannot sustain heterogeneities, except perhaps at the very base of the liquid core.

The ICB corresponds to an increase in P-velocity of about $0.7\ \text{m s}^{-1}$ and an increase in density of about $0.5–1.0 \times 10^3\ \text{kg m}^{-3}$, which indicate a strong depletion in light elements compared to the liquid core. The inner core is rigid, but the S-velocity profile inside the inner core is still poorly known. A lower shear velocity in the uppermost inner core suggests the presence of liquid inclusions. The P-wave quality factor Q_α is low (100–400) with scattered values in the uppermost 300 km. An increase of Q_α with depth is favored by most of the studies, and a rapid change in the characteristics of the attenuation seems to be present at radius ~ 500 km. The relative contributions of anelasticity and scattering in attenuation

are difficult to specify, and anelastic attenuation is probably present both in shear ($1/Q_\mu$) and in bulk ($1/Q_\kappa$).

The inner core is anisotropic in seismic velocities, with to the first approximation a cylindrical anisotropy (transverse isotropy) of 1–3% and a fast axis parallel to the ERA. The uppermost 100–150 km is almost isotropic. Anisotropy in attenuation is also present, with strong attenuation correlated with high velocities in the direction of the ERA. An innermost inner core with radius 300–600 km and an anisotropy different from that in the outer inner core have been detected, but the nature of the anisotropy inside this structure is still debated. It is also a zone of reduced attenuation.

A hemispherical pattern is present in the uppermost 600 km of the inner core, both for uppermost isotropic layer and for anisotropy. In the uppermost 80 km of the isotropic layer, the quasi-eastern hemisphere (40–180° E) has higher velocities and higher attenuation than the western hemisphere. In the depth range 100–600 km, the western hemisphere appears to be more anisotropic than the Eastern one for both P-velocity and attenuation. This dichotomy in anisotropy could be explained either by a variation in the degree of crystal alignment or by a difference in thickness of the isotropic layer, 400 km thick beneath the eastern hemisphere and only 100 km thick beneath the western hemisphere. The correlation between velocity and attenuation, opposite to that observed in the mantle, is best explained by scattering on iron anisotropic crystals or iron grains.

Small-scale lateral heterogeneities inside the inner core are hard to identify unambiguously. At very short wavelengths, scatterers of size 1–10 km have been identified inside the upper part of the inner core and at ICB from the coda of reflected waves. Their characteristics do not seem to be identical everywhere.

A search for a differential rotation of the inner core with respect to the mantle has led to very variable results, depending on the method and data used. Rotation rates from negative (westward rotation) up to more than $1^\circ\,\text{year}^{-1}$ (eastward rotation) have been obtained, large positive values being obtained along a few specific paths involving South Sandwich Island events and null rotation for worldwide analyses. Most of the recent results favor the absence of rotation or very small oscillations, in agreement with the predictions of geodynamic models.

Figure 19 summarizes the main results concerning the core.

1.23.10.2 Open Questions and Future Challenges

The distribution of inner core anisotropy with depth is an important issue. It could help specify the structure of iron in the inner core and how the anisotropy is generated. In parallel, the distribution of attenuation with depth and the S-velocity profile are important pieces of information to specify the texture and to detect partial melting.

The core boundaries are possible places of sedimentation, differentiation, and chemical exchanges that call for refined analyses. In particular, the ICB, which appears as a first-order discontinuity despite the possible presence of a mushy zone, remains to some extent enigmatic. An open question concerns the growing mechanism of the inner core, either from dendrites formed at the ICB or from a 'snow' of iron alloy formed in the lowermost liquid core. The relations between the uppermost inner core and the surrounding dense liquid layer have to be understood. Also, the possibility of liquid core layers with nonzero rigidity and increased viscosity at CMB and ICB deserve further exploration.

The East–West hemispherical pattern, which is a violation of the cylindrical symmetry imposed by the Earth's rotation, must be explained. Other degree-one structures exist in the Earth (e.g., the ocean–continent distribution). The existence of such a pattern in the uppermost inner core, without evidence of compositional heterogeneity, is a puzzling question. A model explaining simultaneously the hemispherical variations in the uppermost isotropic layer, those in anisotropy, and the presence of an innermost inner core has to be found, but a clear image of the inner core structure at depth is still missing.

The debate concerning inner core rotation with respect to the mantle is not completely closed. The origin of the highly varying rotation rates, depending on the method used and on the path considered, has to be understood. The numerous geodynamic problems related to a possible differential rotation or to inner core oscillations require that this question be definitively resolved.

Outside the field of seismology, many constraints are expected from the other domains of physics and chemistry. In particular, the improved performances of experimental and numerical simulations in high-pressure physics will hopefully give new constrains on the phase and texture present at the center of the Earth and on the light elements that could be incorporated in iron. Viscosity of the inner core is also an important parameter to specify, as it is related to thermal convection, deformation ability, and grain size, thus indirectly to anisotropy. On the other hand, geodynamo models including dynamic constraints will give new insights on inner core rotation or oscillations.

Through the different problems presented in this chapter, we have an appraisal of the numerous different fields of physics and chemistry involved in liquid core and inner core structure and dynamics. It seems now very important to favor strong interactions between the concerned scientific communities. This is particularly true for the modeling of the solid–fluid interactions and of the hemispherical pattern.

For seismology, improvements are expected in both observation and modeling. The numerical methods for computing synthetic seismograms in complex structures are important tools that could be more extensively used and that will still evolve. On the other hand, computation of scattered energy in complex media has still to be improved. From the experimental point of view, one of the most drastic problems remains the poor distribution of the data. This is particularly crucial for studying anisotropy, which requires a good sampling in all directions. The large unsampled provinces and the scarcity of polar paths illustrate the importance of maintaining observatories at high latitudes and of developing ocean-bottom observatories. A growing number of seismological studies process signals of very small amplitude, for which stacking is necessary. Permanent small aperture arrays, which are essential for such studies, are still missing at high southern latitudes. Finally, maintaining observatories for decades, despite the considerable effort it represents, is crucial to resolve inner core rotation and more generally to address time-dependent seismology.

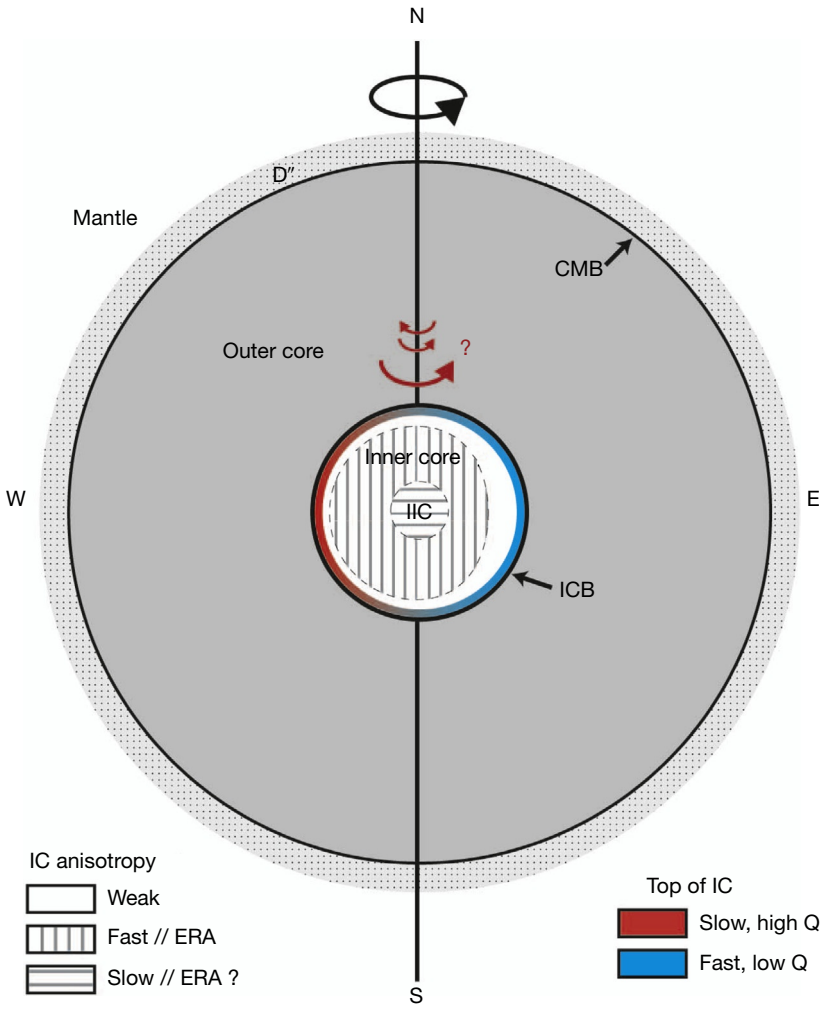

Figure 19 Cartoon of the structure of the core, summarizing the main seismological results: the absence of 3D structure in the liquid core, the existence of a nearly isotropic layer at the top of the inner core with a hemispherical pattern at the very top and a different thickness in each hemisphere, and anisotropy in the body of the inner core with fast axis parallel to the Earth's rotation axis. Still debated (or to specify) are the characteristics of the anisotropy in the innermost inner core and the differential rotation or oscillations of the inner core with respect to the mantle, although a null rotation rate seems now favored. IC, inner core; IIC, innermost inner core; ICB, inner core boundary; CMB, core–mantle boundary; ERA, Earth's rotation axis; Q, P-wave quality factor.

References

Alboussière T, Deguen R, and Melzani M (2010) Melting induced stratification above the Earth's inner core due to convective translation. *Nature* 466: 744–747.

Alexandrakis C and Eaton DW (2010) Precise seismic-wave velocity atop Earth's core: No evidence for outer-core stratification. *Physics of the Earth and Planetary Interiors* 180: 59–65.

Alfè D, Gillan M, and Price GD (2003) Thermodynamics from first principles: Temperature and composition of the Earth's core. *Mineralogical Magazine* 67: 113–123.

Andrault D, Bolfan-Casanova N, Ohtaka O, et al. (2009) Melting diagrams of Fe-rich alloys determined from synchrotron in situ measurements in the 15–23 GPa pressure range. *Physics of the Earth and Planetary Interiors* 174: 181–191.

Andrews J, Deuss A, and Woodhouse J (2006) Coupled normal-mode sensitivity to inner-core shear velocity and attenuation. *Geophysical Journal International* 167: 204–212.

Aubert J (2013) Flow throughout the Earth's core inverted from geomagnetic observations and numerical dynamo models. *Geophysical Journal International* 192: 537–556.

Aubert J, Amit H, Hulot G, and Olson P (2008) Thermochemical flows couple the Earth's inner core growth to mantle heterogeneity. *Nature* 454: 758–761.

Aubert J and Dumberry M (2011) Steady and fluctuating inner core rotation in numerical geodynamo models. *Geophysical Journal International* 184: 162–170.

Aurnou J, Brito D, and Olson P (1996) Mechanisms of inner core super-rotation. *Geophysical Research Letters* 23: 3401–3404.

Badro J, Fiquet G, Guyot F, et al. (2007) Effect of light elements on the sound velocities in solid iron: Implications for the composition of Earth's core. *Earth and Planetary Science Letters* 254: 233–238.

Beghein C and Trampert J (2003) Robust normal mode constraints on inner core anisotropy from model space search. *Science* 299: 552–555.

Belonoshko AB, Skorodumova NV, Davis S, Osiptsov AN, Rosengren A, and Johansson B (2007) Origin of the low rigidity of the Earth's inner core. *Science* 316: 1603–1605.

Bergman MI (1997) Measurements of elastic anisotropy due to solidification texturing and the implications for the Earth's inner core. *Nature* 389: 60–63.

Bergman MI (1998) Estimates of the Earth's inner core grain size. *Geophysical Research Letters* 25: 1593–1596.

Bergman MI, Agrawal S, Carter M, and Macleod-Silberstein M (2003) Transverse solidification textures in hexagonal close-packed alloys. *Journal of Crystal Growth* 255: 204–211.

Bergman MI, Cole DM, and Jones JR (2002) Preferred crystal orientations due to melt convection during directional solidification. *Journal of Geophysical Research* 107: ECV 6-1–6-8.

Bergman MI, Lewis DJ, Myint IH, Slivka L, Karato SI, and Abreu A (2010) Grain growth and loss of texture during annealing of alloys, and the translation of Earth's inner core. *Geophysical Research Letters* 37: L22313.
Bhattacharyya J, Shearer P, and Masters G (1993) Inner core attenuation from short-period PKP(BC) versus PKP(DF) waveforms. *Geophysical Journal International* 114: 1–11.
Birch F (1952) Elasticity and constitution of the Earth's interior. *Journal of Geophysical Research* 57: 227.
Birch F (1964) Density and composition of mantle and core. *Journal of Geophysical Research* 69: 4377–4388.
Bolt BA (1962) Gutenberg's PKP early observations. *Nature* 196: 122–124.
Bolt BA (1977) The detection of PKIIKP and damping in the inner core. *Annali di Geofisica* 30: 507–520.
Bolt BA (1982) *Inside the Earth*. San Francisco, CA: Freeman.
Bolt BA and Qamar A (1970) Upper bound to the density jump at the boundary of the Earth's inner core. *Nature* 228: 148–150.
Bormann P, Klinge K, and Wendt S (2002) Chapter 11: Data analysis and seismogram interpretation. In: Bormann P (ed.) *IASPEI New Manual of Seismological Observatory Practice*, vol. 1, p. 102. Potsdam: GeoForschungsZentrum.
Bowers D, McCormack DA, and Sharrock DS (2000) Observations of PKP(DF) and PKP(BC) across the United Kingdom: Implications for studies of attenuation in the earth's core. *Geophysical Journal International* 140: 374–384.
Bréger L, Romanowicz B, and Rousset S (2000a) New constraints on the structure of the inner core from P′P′. *Geophysical Research Letters* 17: 2781–2784.
Bréger L, Romanowicz B, and Tkalčić H (1999) PKP(BC-DF) travel time residuals and short scale heterogeneity in the deep Earth. *Geophysical Research Letters* 26: 3169–3172.
Bréger L, Tkalčić H, and Romanowicz B (2000b) The effect of D″ on PKP(AB-DF) travel time residuals and possible implications for inner core structure. *Earth and Planetary Science Letters* 175: 133–143.
Brush SG (1980) Discovery of the Earth's core. *American Journal of Physics* 48: 705–724.
Buffett BA (1997) Geodynamic estimates of the viscosity of the Earth's inner core. *Nature* 338: 571–573.
Buffett BA (2000) Dynamics of the Earth's core. In: *Earth's Deep Interior: Mineral Physics and Tomography from the Atomic to the Global Scale*. *AGU Geophysical Monograph*, vol. 117, pp. 37–62. Washington, DC: American Geophysical Union.
Buffett BA (2009) Onset and orientation of convection in the inner core. *Geophysical Journal International* 179: 711–719.
Buffett BA, Garnero EL, and Jeanloz R (2010) Sediments at the top of Earth's core. *Science* 290: 1338–1342.
Buffett BA and Glatzmaier GA (2000) Gravitational breaking of inner core rotation in geodynamo simulations. *Geophysical Research Letters* 27: 3125–3128.
Buffett BA and Seagle CT (2010) Stratification of the top of the core due to chemical interactions with the mantle. *Journal of Geophysical Research* 115: B04407.
Buffett BA and Wenk HR (2004) Texturing of the Earth's inner core by Maxwell stresses. *Nature* 413: 60–63.
Bullen K (1940) The problem of the Earth's density variation. *Bulletin of the Seismological Society of America* 30: 235–250.
Bullen KE and Haddon RAW (1973) The ellipticities of surfaces of equal density inside the Earth. *Physics of the Earth and Planetary Interiors* 7: 199–202.
Busse FH (1975) A model of the geodynamo. *Geophysical Journal of the Royal Astronomical Society* 42: 437–459.
Calvet M, Chevrot S, and Souriau A (2006) P-wave propagation in transversely isotropic media. II. Application to inner core anisotropy: Effects of data merging, parametrization and a priori information. *Physics of the Earth and Planetary Interiors* 156: 21–40.
Calvet M and Margerin L (2008) Constraints on the grain size and stable iron phases in the uppermost inner core from multiple scattering modeling of seismic velocity and attenuation. *Earth and Planetary Science Letters* 156: 21–40.
Cao A, Masson Y, and Romanowicz B (2007) Short wavelength topography on the inner core boundary. *PNAS* 104: 31–35.
Cao A and Romanowicz B (2004a) Constraints on density and shear velocity contrasts at the inner core boundary. *Geophysical Journal International* 157: 1–6.
Cao A and Romanowicz B (2004b) Hemispherical transition of seismic attenuation at the top of the earth's inner core. *Earth and Planetary Science Letters* 228: 243–253.
Cao A and Romanowicz B (2007) Test of the innermost inner core models using broadband PKIKP travel time residuals. *Geophysical Research Letters* 34: L08303.
Cao A and Romanowicz B (2009) Constraints on shear wave attenuation in the Earth's inner core from an observation of PKJKP. *Geophysical Research Letters* 36: L09301.
Cao A, Romanowicz B, and Takeuchi N (2005) An observation of PKJKP: Inferences on inner core shear properties. *Science* 308: 1453–1455.
Carcione JM and Cavallini F (1994) A rheological model for anelastic anisotropic media with applications to seismic wave propagation. *Geophysical Journal International* 119: 338–348.
Choy GL (1977) Theoretical seismograms of core phases calculated by frequency-dependent full wave theory, and their interpretation. *Geophysical Journal of the Royal Astronomical Society* 51: 275–312.
Choy GL and Cormier VF (1983) The structure of the inner core inferred from short-period and broadband GDSN data. *Geophysical Journal of the Royal Astronomical Society* 72: 1–21.
Choy GL and Richards PG (1975) Pulse distortion and Hilbert transformation in multiply reflected and refracted body waves. *Bulletin of the Seismological Society of America* 65: 55–70.
Cleary J and Haddon RAW (1972) Seismic wave scattering near the core-mantle boundary: A new interpretation of precursors of PKP. *Nature* 240: 549–551.
Collier JD and Helffrich G (2001) Estimate of inner core rotation rate from United Kingdom regional seismic network data and consequences for inner core dynamical behaviour. *Physics of the Earth and Planetary Interiors* 193: 523–537.
Cormier VF (1981) Short-period PKP phases and the anelastic mechanism of the inner core. *Physics of the Earth and Planetary Interiors* 24: 291–301.
Cormier VF (2007) Texture of the uppermost inner core from forward- and backscattered seismic waves. *Earth and Planetary Science Letters* 258: 442–453.
Cormier VF (2009) A glassy lowermost outer core. *Geophysical Journal International* 179: 374–380.
Cormier VF, Attanayake J, and He K (2011) Inner core freezing and melting: Constraints from seismic body waves. *Physics of the Earth and Planetary Interiors* 188: 163–172.
Cormier VF and Choy GL (1986) A search for lateral heterogeneity in the inner core from differential travel times near PKP-D and PKP-C. *Geophysical Research Letters* 13: 1553–1556.
Cormier VF and Li X (2002) Frequency-dependent seismic attenuation in the inner core. 2. A scattering and fabric interpretation. *Journal of Geophysical Research* 107(B12): 2362.
Cormier VF, Li X, and Choy GL (1998) Seismic attenuation of the inner core: Viscoelastic or stratigraphic? *Geophysical Research Letters* 25: 4019–4022.
Cormier VF and Richards PG (1976) Comments on "The damping of core waves" by Antony Qamar and Alfredo Eisenberg. *Journal of Geophysical Research* 81: 3066–3068.
Cormier VF and Stroujkova A (2005) Waveform search for the innermost inner core. *Earth and Planetary Science Letters* 236: 96–105.
Cottaar S and Buffett B (2012) Convection in the Earth's inner core. *Physics of the Earth and Planetary Interiors* 198: 67–78.
Creager KC (1992) Anisotropy in the inner core from differential travel times of the phases PKP and PKIKP. *Nature* 356: 309–314.
Creager KC (1997) Inner core rotation rate from small scale heterogeneity and time-varying travel times. *Science* 278: 1284–1288.
Creager KC (1999) Large-scale variations in inner core anisotropy. *Journal of Geophysical Research* 104: 23127–23139.
Creager KC (2000) Inner core anisotropy and rotation. In: Dehant V, et al. (eds.) *Core Dynamics, Structure and Rotation*. *American Geodynamic Series*, vol. 31, pp. 89–114. Washington, DC: American Geophysical Union.
Creager KC and Jordan TH (1986) Aspherical structure of the core–mantle boundary from PKP travel times. *Geophysical Research Letters* 13: 1497–1500.
Crossley DJ, Rochester M, and Peng Z (1992) Slichter modes and Love numbers. *Geophysical Research Letters* 19: 1679–1682.
Cummins P and Johnson L (1988a) Synthetic seismograms for an inner core transition of finite thickness. *Geophysical Journal* 94: 21–34.
Cummins P and Johnson L (1988b) Short-period body wave constraints on the properties of the Earth's inner core boundary. *Journal of Geophysical Research* 93: 9058–9074.
Dai Z, Wang W, and Wen L (2012) Irregular topography at the Earth's inner core boundary. *PNAS* 109: 7654–7658.
Defraigne P, Dehant V, and Wahr JM (1996) Internal loading of an inhomogeneous compressible earth with phase boundaries. *Geophysical Journal International* 125: 173–192.
Deguen R (2012) Structure and dynamics of Earth's inner core. *Earth and Planetary Science Letters* 333–334: 211–225.
Deguen R, Alboussière T, and Brito D (2007) On the presence and structure of a mush at the inner core boundary of the Earth. *Physics of the Earth and Planetary Interiors* 274: 1887–1891.
Deguen R and Cardin P (2009) Tectonic history of the Earth's inner core preserved in its seismic structure. *Nature Geoscience* 2: 419–422.
Deguen R and Cardin P (2011) Thermo-chemical convection in Earth's inner core. *Geophysical Journal International* 187: 1101–1118.

Deparis V and Legros H (2002) *Voyage à l'intérieur de la Terre*, 627 pp. Paris: CNRS Edition.

Deuss A (2008) Normal mode constraints on shear and compressional wave velocity of the Earth's inner core. *Earth and Planetary Science Letters* 268: 365–375.

Deuss A, Woodhouse JH, Paulssen H, and Trampert J (2000) The observation of inner core shear waves. *Geophysical Journal International* 142: 67–73.

Doornbos DJ (1974) The anelasticity of the inner core. *Geophysical Journal of the Royal Astronomical Society* 38: 397–415.

Doornbos DJ (1983) Observable effects of the seismic absorption band in the Earth. *Geophysical Journal of the Royal Astronomical Society* 75: 693–711.

Doornbos DJ and Hilton T (1989) Models of core–mantle boundary and the travel times of internally reflected core phases. *Journal of Geophysical Research* 94: 15741–15751.

Durek JJ and Romanowicz B (1999) Inner core anisotropy inferred by direct inversion of normal mode spectra. *Geophysical Journal International* 139: 599–622.

Dziewonski AM and Anderson DL (1981) Preliminary reference earth model. *Physics of the Earth and Planetary Interiors* 25: 297–356.

Dziewonski AM and Gilbert F (1971) Solidity of the inner core of the Earth inferred from normal mode oscillations. *Nature* 234: 465.

Earle PS and Shearer PM (1997) Observations of PKKP precursors used to estimate small-scale topography on the core-mantle boundary. *Science* 277: 667–670.

Eaton DW and Kendall JM (2006) Improving seismic resolution of outermost core structure by multichannel analysis and deconvolution of broadband SmKS phases. *Physics of the Earth and Planetary Interiors* 155: 104–119.

Emmerich H (1993) Theoretical study of the influence of CMB topography on the core reflections ScS. *Physics of the Earth and Planetary Interiors* 80: 125–134.

Engdahl ER, Van der Hilst R, and Buland RP (1998) Global teleseismic earthquake relocation with improved travel times and procedures for depth determination. *Bulletin of the Seismological Society of America* 88: 722–743.

Fearn DR, Loper DE, and Roberts PH (1981) Structure of the Earth's inner core. *Nature* 292: 232–233.

Forte AM, Mitrovica JX, and Woodward RL (1995) Seismic-geodynamic determination of the origin of excess ellipticity of the core–mantle boundary. *Geophysical Research Letters* 22: 1013–1016.

Garcia R (2002a) Constraints on upper inner core structure from waveform inversion of core phases. *Geophysical Journal International* 150: 651–664.

Garcia R (2002b) Seismological and mineral constraints on the inner core fabric. *Geophysical Research Letters* 29: 1958.

Garcia R and Souriau A (2000a) Amplitude of core–mantle boundary estimated by stochastic analysis of core phases. *Physics of the Earth and Planetary Interiors* 117: 345–359.

Garcia R and Souriau A (2000b) Inner core anisotropy and heterogeneity level. *Geophysical Research Letters* 27: 3121–3124; Correction (2001) *Geophysical Research Letters* 28: 85.

Garcia R, Tkalčić H, and Chevrot S (2006) A new global PKP data set to study Earth's core and deep mantle. *Physics of the Earth and Planetary Interiors* 159: 15–31.

Garnero EJ, Helmberger DV, and Grand SP (1993) Constraining outermost core velocity with SmKS waves. *Geophysical Research Letters* 25: 2341–3344.

Garnero EJ and Lay T (1998) Effects of D″ anisotropy on seismic velocity models of the outermost core. *Geophysical Research Letters* 20: 2463–2466.

Geballe ZM, Lasbleis M, Cormier VF, and Day EA (2013) Sharp hemisphere boundaries in a translating inner core. *Geophysical Research Letters* 40: 1719–1723. http://dx.doi.org/10.1002/grl.50372.

Glatzmaier GA and Roberts PH (1996) Rotation and magnetism of Earth's inner core. *Science* 274: 1887–1891.

Greff-Lefftz M and Legros H (1996) Viscoelastic mantle density heterogeneity and core–mantle boundary topography. *Geophysical Journal International* 125: 567–576.

Gubbins D (1981) Rotation of the inner core. *Journal of Geophysical Research* 86: 11695–11699.

Gubbins D, Alfè D, and Davies CJ (2013) Compositional instability of Earth's solid inner core. *Geophysical Research Letters* 40: 1–5.

Gubbins D, Masters G, and Nimmo F (2008) A thermochemical boundary layer at the base of the Earth's outer core and independent estimate of core heat flux. *Geophysical Journal International* 174: 1007–1018.

Gubbins D, Sreenivasan B, Bound J, and Rost S (2011) Melting of the Earth's inner core. *Nature* 473: 361–363.

Gutenberg B (1913) Uber die Konstitution des Erdinnern, erschlossen aus Erdbebenbeobachtungen. *Physikalische Zeitschrift* 14: 1217.

Gwinn CR, Herring TA, and Shapiro II (1986) Geodesy by radio interferometry: Studies of the forced nutations of the Earth: 2. Interpretation. *Journal of Geophysical Research* 91: 4755–4765.

Häge H (1983) Velocity constraints for the inner core inferred from long period PKP amplitudes. *Physics of the Earth and Planetary Interiors* 31: 171–185.

Helffrich G and Kaneshima S (2004) Seismological constraints on core composition from Fe–O–S liquid immiscibility. *Science* 306: 2239–2242.

Helffrich G and Kaneshima S (2010) Outer-core compositional stratification from observed core wave speed profile. *Nature* 468: 807–811.

Hirose K, Labrosse S, and Hernlund J (2013) Composition and state of the core. *Annual Review of Earth and Planetary Sciences* 41: 25.1–25.35.

Iritani R, Takeuchi N, and Kawakatsu H (2010) Seismic attenuation structure of the top half of the inner core beneath the northeastern Pacific. *Geophysical Research Letters* 37: L19303.

Irving JCE and Deuss A (2011a) Stratified anisotropic structure at the top of Earth's inner core: A normal mode study. *Physics of the Earth and Planetary Interiors* 186: 59–69.

Irving JCE and Deuss A (2011b) Hemispherical structure in inner core velocity anisotropy. *Journal of Geophysical Research* 116: B04307.

Irving JCE, Deuss A, and Woodhouse JH (2009) Normal mode coupling due to hemispherical anisotropic structure in Earth's inner core. *Geophysical Journal International* 178: 962–975.

Ishii M and Dziewonski AM (2002) The innermost inner core of the Earth: Evidence for a change in anisotropic behaviour at the radius of about 300 km. *PNAS* 99: 14026–14030.

Ishii M and Dziewonski AM (2003) Distinct seismic anisotropy at the centre of the Earth. *Physics of the Earth and Planetary Interiors* 140: 203–217.

Ishii M and Dziewonski AM (2005) Constraints on the outer core tangent cylinder using normal-mode splitting measurements. *Geophysical Journal International* 162: 787–792.

Ishii M, Dziewonski AM, Tromp J, and Ekström G (2002a) Joint inversion of normal mode and body wave data for inner core anisotropy 2. Possible complexities. *Journal of Geophysical Research* 107: 2380.

Ishii M, Tromp J, Dziewonski AM, and Ekström G (2002b) Joint inversion of normal mode and body wave data for inner core anisotropy 1. Laterally homogeneous anisotropy. *Journal of Geophysical Research* 107: 2379.

Isse T and Nakanishi I (2002) Inner-core anisotropy beneath Australia and differential rotation. *Geophysical Journal International* 151: 255–263.

Ivan M and Moloto-A-Kenguemba GR (2007) Attenuation in the uppermost inner core from PKP recordings at African seismological stations. *Studia Geophysica et Geodetica* 51: 221–230.

Jacobs JA (1953) The Earth's inner core. *Nature* 172: 297.

Jeanloz R and Wenk HR (1988) Convection and anisotropy of the inner core. *Geophysical Research Letters* 15: 72–75.

Jeffreys H (1926) The rigidity of the Earth's central core. *Monthly Notices of the Royal Astronomical Society* 1: 371.

Jephcoat A and Olson P (1987) Is the inner core of the Earth pure iron? *Nature* 325: 332–335.

Julian BR, Davies D, and Sheppard RM (1972) PKJKP. *Nature* 235: 317–318.

Kampfman W and Müller G (1989) PcP amplitude calculations for a core–mantle boundary with topography. *Geophysical Research Letters* 16: 653–656.

Kaneshima S (1996) Mapping heterogeneity of the uppermost inner core using two pairs of core phases. *Geophysical Research Letters* 23: 3075–3078.

Karato S (1993) Inner core anisotropy due to the magnetic field-induced preferred orientation of iron. *Science* 262: 1708–1710.

Karato S (1999) Maxwell stress-induced flow in the Earth's inner core: Implications for seismic anisotropy and geodynamo. *Nature* 402: 871–873.

Kawakatsu H (1992) Some attempt to observe PKJKP. *Central Core of the Earth* 2: 53–56 (in Japanese).

Kawakatsu H (2006) Sharp and seismically transparent inner core boundary region revealed by an entire network observation of near vertical PKiKP. *Earth, Planets and Space* 58: 855–863.

Kazama T, Kawakatsu H, and Takeuchi N (2008) Depth-dependent attenuation structure of the inner core inferred from short-period Hi-net data. *Physics of the Earth and Planetary Interiors* 167: 155–160.

Kennett BLN (1998) On the density distribution within the Earth. *Geophysical Journal International* 132: 374–382.

Kennett BLN and Engdahl ER (1991) Traveltimes for global earthquake location and phase identification. *Geophysical Journal International* 105: 429–465.

Kennett BLN, Engdahl ER, and Buland R (1995) Constraints on seismic velocities in the Earth from travel times. *Geophysical Journal International* 122: 108–124.

Koelemeijer PJ, Deuss A, and Trampert J (2012) Normal mode sensitivity to Earth's D″ layer and topography on the core-mantle boundary: What we can and cannot see. *Geophysical Journal International* 190: 553–568.
Kohler M (1997) Three-dimensional velocity structure and resolution of the core–mantle boundary region from whole mantle-inversion of body waves. *Physics of the Earth and Planetary Interiors* 101: 85–104.
Koot L, Dumberry M, Rivoldini A, de Viron O, and Dehant V (2010) Constraints on the coupling at the core–mantle and inner core boundaries inferred from nutation observations. *Geophysical Journal International* 182: 1279–1294.
Koper KD and Dombrovskaya M (2005) Seismic properties of the inner core boundary from PKiKP/P amplitude ratios. *Earth and Planetary Science Letters* 237: 680–694.
Koper KD, Franks JM, and Dombrovskaya M (2004) Evidence for small-scale heterogeneity in Earth's inner core from a global study of PKiKP coda waves. *Earth and Planetary Science Letters* 228: 227–241.
Koper KD and Pyle ML (2004) Observation of PKiKP/PcP amplitude ratios and implications for Earth structure at the boundaries of the liquid core? *Journal of Geophysical Research* 109: B03301.
Koper KD, Pyle ML, and Franks JM (2003) Constraints on aspherical core structure from PKiKP-PcP differential travel times. *Journal of Geophysical Research* 108: 2168–2180.
Krasnoshchekov DN, Kaaziz PB, and Ovtchinnikov VM (2005) Seismological evidence for mosaic structure of the surface of the Earth's inner core. *Nature* 435: 483–487.
Kuwayama Y, Hirose K, Sata N, and Oshihi Y (2008) Phase relation of iron and iron-nickel alloys up to 300 GPa: Implications for composition and structure of the Earth's inner core. *Earth and Planetary Science Letters* 273: 379–385.
Laske G and Masters G (1999) Limits on differential rotation of the inner core from an analysis of the Earth's free oscillations. *Nature* 402: 66–68.
Laske G and Masters G (2003) The Earth's free oscillations and the differential rotation of the inner core. In: Dehant V, et al. (eds.) *Earth's Core, Dynamics, Structure, Rotation*. *Geodynamics Series*, vol. 31, pp. 5–22. Washington, DC: American Geophysical Union.
Lassak TM, McNamara AK, Garnero EJ, and Zhong S (2010) Core–mantle boundary topography as a possible constraint on lower mantle chemistry and dynamics. *Earth and Planetary Science Letters* 289: 232–241.
Lay T and Young CJ (1990) The stably stratified outermost core revisited. *Geophysical Research Letters* 17: 2001–2004.
Lehmann I (1936) P′. *Bureau Central Seismologique International, Strasbourg, Travaux Scientifiques A* 14: 3–31.
Leyton F and Koper KD (2007a) Using PKiKP coda to determine inner core structure: 1. Synthesis of coda envelopes using single-scattering theories. *Journal of Geophysical Research* 112: B05316.
Leyton F and Koper KD (2007b) Using PKiKP coda to determine inner core structure: 2. Determination of Q_C. *Journal of Geophysical Research* 112: B05317.
Leyton F, Koper KD, Zhu L, and Dombrovskaya M (2005) On the lack of seismic discontinuities within the inner core. *Geophysical Journal International* 162: 779–786.
Li X and Cormier VF (2002) Frequency dependent seismic attenuation in the inner core. 1. A viscoelastic interpretation. *Journal of Geophysical Research* 107(B12): 2361.
Li X, Giardini D, and Woodhouse JH (1991) Large-scale three-dimensional even-degree structure of the Earth from splitting of long-period normal modes. *Journal of Geophysical Research* 96: 551–577.
Li A and Richards PG (2003a) Using earthquake doublets to study inner core rotation and seismicity catalog precision. *Geochemistry, Geophysics, Geosystems* 4: 1072.
Li A and Richards PG (2003b) Study of inner core structure and rotation using seismic records from Novaya Zemlya underground nuclear tests. In: Dehant V, et al. (eds.) *Earth's Core, Dynamics, Structure, Rotation*. *Geodynamics Series*, vol. 31, pp. 23–30. Washington, DC: American Geophysical Union.
Lindner D, Song X, Ma P, and Christensen DH (2010) Inner core rotation and its variability from nonparametric modeling. *Journal of Geophysical Research* 115: B04307.
Lister JR and Buffett BA (1998) Stratification of the outer core at the core–mantle boundary. *Physics of the Earth and Planetary Interiors* 105: 5–19.
Loper DE and Roberts PH (1981) A study of conditions at the inner core boundary of the Earth. *Physics of the Earth and Planetary Interiors* 24: 302–307.
Mäkinen A and Deuss A (2011) Global seismic body wave observations of temporal variations in the Earth's inner core, and implications for its differential rotation. *Geophysical Journal International* 187: 355–370.
Mäkinen A and Deuss A (2013) Normal mode splitting function measurements of anelasticity and attenuation in the Earth's inner core. *Geophysical Journal International* 194: 401–416. http://dx.doi.org/10.1093/gji/ggt092.
Masters G (1979) Observational constraints on the chemical and thermal structure of the earth's deep interior. *Geophysical Journal of the Royal Astronomical Society* 57: 507–534.
Masters G and Gilbert F (1981) Structure of the inner core inferred from observations of its spheroidal shear modes. *Geophysical Research Letters* 8: 569–571.
Masters G and Gubbins D (2003) On the resolution of density within the Earth. *Physics of the Earth and Planetary Interiors* 140: 159–167.
Mathews PM, Herring TA, and Buffett B (2002) Modeling of nutation and precession: New nutation series for nonrigid Earth and insights into the Earth's interior. *Journal of Geophysical Research* 107(B4): 2068.
McSweeney TJ, Creager KC, and Merrill RT (1997) Depth extent of inner-core seismic anisotropy and implications for geomagnetism. *Physics of the Earth and Planetary Interiors* 101: 131–156.
Menke W (1986) Few 2–50 km corrugation on the core–mantle boundary. *Geophysical Research Letters* 13: 1501–1504.
Miller MS, Niu F, and Vanacore EA (2013) Aspherical structure heterogeneity within the uppermost inner core: Insights into the hemispherical boundaries and core formation. *Physics of the Earth and Planetary Interiors* 223: 8–20.
Mizzon H and Monnereau M (2013) Implication of the lopsided growth for the viscosity of Earth's inner core. *Earth and Planetary Science Letters* 361: 391–401.
Mochizuki E and Ohminato T (1989) On the anomalous splitting of Earth's free oscillations. *Geophysical Research Letters* 16: 1415–1416.
Monnereau M, Calvet M, Margerin L, and Souriau A (2010) Lopsided growth of Earth's inner core. *Science* 328: 1014–1017.
Montagner J-P and Kennett BLN (1995) How to reconcile body-wave and normal mode reference Earth's models? *Geophysical Journal International* 125: 229–248.
Morelli A and Dziewonski AM (1987) Topography of the core–mantle boundary and lateral homogeneity of the liquid core. *Nature* 325: 678–683.
Morelli A and Dziewonski AM (1993) Body wave traveltimes and a spherically symmetric P- and S-wave velocity model. *Geophysical Journal* 112: 178–194.
Morelli A, Dziewonski AM, and Woodhouse JH (1986) Anisotropy of the inner core inferred from PKIKP travel times. *Geophysical Research Letters* 13: 1545–1548.
Müller G (1973) Amplitude studies of core phases. *Journal of Geophysical Research* 78: 3469–3490.
Niazi M and Johnson LR (1992) Q in the inner core. *Physics of the Earth and Planetary Interiors* 74: 55–62.
Niu F and Chen Q-F (2008) Seismic evidence for distinct anisotropy in the innermost inner core. *Nature Geoscience* 1: 692–696.
Niu F and Wen L (2001) Hemispherical variations in seismic velocity at the top of the Earth's inner core. *Nature* 410: 1081–1084.
O'Connell R and Budianski B (1977) Viscoelastic properties of fluid-saturated cracked solids. *Journal of Geophysical Research* 82: 5719–5735.
Obayashi M and Fukao Y (1997) P and PcP travel time tomography for the core–mantle boundary. *Journal of Geophysical Research* 102: 17825–17841.
Ohtaki T, Kaneshima S, and Kanjo K (2012) Seismic structure near the inner core boundary in the south polar region. *Journal of Geophysical Research* 117: B03312.
Okal E and Cansi Y (1998) Detection of PKJKP at intermediate periods by progressive multichannel correlation. *Earth and Planetary Science Letters* 164: 23–30.
Oldham RD (1906) The constitution of the interior of the Earth as revealed by earthquakes. *Quarterly Journal of the Geological Society of London* 62: 456.
Olson P and Deguen R (2012) Eccentricity of the geomagnetic dipole caused by lopsided inner core growth. *Nature Geoscience* 5: 565–569.
Oreshin SI and Vinnik LP (2004) Heterogeneity and anisotropy of seismic attenuation in the inner core. *Geophysical Research Letters* 31: L02613.
Ouzounis A and Creager KC (2001) Isotropy overlying anisotropy at the top of the inner core. *Geophysical Research Letters* 28: 4331–4334.
Palmer A and Smylie D (2005) VLBI observations of free core nutations and viscosity at the top of the core. *Physics of the Earth and Planetary Interiors* 148: 285–301.
Peacock S and Hudson JA (1990) Seismic properties of rocks with distribution of small cracks. *Geophysical Journal International* 102: 471–484.
Peng Z, Koper KD, Vidale JE, Leyton F, and Shearer P (2008) Inner-core fine-scale structure from scattered waves recorded by LASA. *Journal of Geophysical Research* 113: B09312.
Piersanti A, Boschi L, and Dziewonski AM (2001) Estimating lateral structure inside the Earth's outer core. *Geophysical Research Letters* 28: 1659–1662.
Poirier JP (1988) Transport properties of liquid metals and viscosity of the Earth's core. *Geophysical Journal International* 92: 99–105.
Poirier JP (1994) Light elements in the Earth's outer core – A critical review. *Physics of the Earth and Planetary Interiors* 85: 319–337.
Poirier JP and Price GD (1999) Primary slip system of ε-iron and anisotropy of the Earth's inner core. *Physics of the Earth and Planetary Interiors* 110: 147–156.

Poirier JP and Shankland TJ (1993) Dislocation melting of iron and the temperature of the inner core boundary, revisited. *Geophysical Journal International* 115: 147–151.

Poupinet G, Ellsworth WL, and Fréchet J (1984) Monitoring velocity variation in the crust using earthquake doublet: An application to the Calaveras fault, California. *Journal of Geophysical Research* 89: 5719–5731.

Poupinet G and Kennett BLN (2004) On the observation of high frequency PKiKP and its coda in Australia. *Physics of the Earth and Planetary Interiors* 146: 497–511.

Poupinet G, Pillet R, and Souriau A (1983) Possible heterogeneity in the Earth's core deduced from PKIKP travel times. *Nature* 305: 204–206.

Poupinet G, Souriau A, and Coutant O (2000) The existence of an inner core super-rotation questioned by teleseismic doublets. *Physics of the Earth and Planetary Interiors* 118: 77–88.

Pulliam RJ and Stark PB (1993) Bumps on the core–mantle boundary: Are they facts or artefacts? *Journal of Geophysical Research* 98: 1943–1955.

Qamar A and Eisenberg A (1974) The damping of core waves. *Journal of Geophysical Research* 79: 758–765.

Rekdal T and Doornbos DJ (1992) The times and amplitudes of core phases for a variable core–mantle boundary layer. *Geophysical Journal International* 108: 546–556.

Ritzwoller MH, Masters G, and Gilbert F (1986) Observations of anomalous splitting and their interpretation in terms of aspherical structure. *Journal of Geophysical Research* 91: 10203–10228.

Rodgers A and Wahr J (1993) Inference of core-mantle boundary topography from ISC PcP and PKP traveltimes. *Geophysical Journal International* 115: 991–1011.

Romanowicz B and Bréger L (2000) Anomalous splitting of free oscillations: A reevaluation of possible interpretations. *Journal of Geophysical Research* 105: 21559–21578.

Romanowicz B and Durek JJ (2000) Seismological constraints on attenuation in the Earth: A review. In: Karato S-I, et al. (ed.) *Earth's Deep Interior: Mineral Physics and Tomography from the Atomic to the Global Scale. AGU Geophysical Monograph*, vol. 117, pp. 161–180. Washington, DC: American Geophysical Union.

Romanowicz B, Li XD, and Durek JJ (1996) Anisotropy in the inner core: Could it be due to low-order convection? *Science* 274: 963–966.

Romanowicz B, Tkalčić H, and Bréger L (2003) On the origin of complexity in PKP travel time data. In: Dehant V, et al. (eds.) *Earth's Core Dynamics, Structure and Rotation. AGU Geodynamics Series*, vol. 31, pp. 31–44. Washington, DC: American Geophysical Union.

Rosat S, Rogister Y, Crossley D, and Hinderer J (2006) A search for the Slichter triplet with superconducting gravimeters: Impact of the density jump at the inner core boundary. *Journal of Geodynamics* 41: 296–306.

Rost S and Revenaugh J (2001) Seismic detection of rigid zones at the top of the core. *Science* 294: 1911–1914.

Rost S and Revenaugh J (2004) Small-scale changes of core–mantle boundary reflectivity studied using core reflected PcP. *Physics of the Earth and Planetary Interiors* 145: 19–36.

Sato S, Fehler MC, and Maeda T (2012) *Seismic Wave Propagation and Scattering in the Heterogeneous Earth*, 2nd edn. Berlin: Springer.

Sharrock DS and Woodhouse JH (1998) Investigation of time dependent inner core structure by the analysis of free-oscillation spectra. *Earth, Planets and Space* 50: 1013–1018.

Shearer P (1994) Constraints on inner core anisotropy from PKP(DF) travel times. *Journal of Geophysical Research* 99: 19647–19659.

Shearer P, Hedlin MAH, and Earle PS (1998) PKP and PKKP precursor observations: Implications for the small-scale structure of the deep mantle and core. In: *The Core Mantle Boundary Region. Geodynamics Series*, vol. 28, pp. 37–55. Washington, DC: American Geophysical Union.

Shearer P and Masters G (1990) The density and shear velocity contrast at the inner core boundary. *Geophysical Journal International* 102: 491–498.

Shearer PM, Rychert CA, and Liu Q (2011) On the visibility of the inner-core shear wave phase PKJKP at long periods. *Geophysical Journal International* 185: 1379–1383.

Shearer PM, Toy KM, and Orcutt JA (1988) Axi-symmetric Earth models and inner core anisotropy. *Nature* 333: 228–232.

Shimizu H, Poirier JP, and Le Mouël JL (2005) On crystallization at the inner core boundary. *Physics of the Earth and Planetary Interiors* 151: 37–51.

Singh S, Taylor MAJ, and Montagner JP (2000) On the presence of liquid in Earth's inner core. *Science* 287: 2471–2474.

Smylie DE (1999) Viscosity near Earth's solid inner core. *Science* 284: 461–463.

Soldati G, Boschi L, and Forte AM (2012) Tomography of core–mantle boundary and lowermost mantle coupled by geodynamics. *Geophysical Journal International* 180: 730–746.

Song X (1996) Anisotropy in central part of inner core. *Journal of Geophysical Research* 101: 16089–16097.

Song X (2000) Joint inversion for inner core rotation, inner core anisotropy, and mantle heterogeneity. *Journal of Geophysical Research* 105: 7931–7943.

Song X (2003) Three-dimensional structure and differential rotation of the inner core. In: Dehant V, et al. (eds.) *Earth's Core, Dynamics, Structure and Rotation. Geophysical Monograph Geodynamics Series*, vol. 31, pp. 45–63. Washington, DC: American Geophysical Union.

Song X and Dai W (2008) Topography of Earth's inner core boundary from high-quality waveform doublets. *Geophysical Journal International* 175: 386–399.

Song X and Helmberger DV (1992) Velocity structure near the inner core boundary from waveform modeling. *Journal of Geophysical Research* 97: 6573–6586.

Song X and Helmberger DV (1995a) A P wave velocity model of the Earth's core. *Journal of Geophysical Research* 100: 9817–9830.

Song X and Helmberger DV (1995b) Depth dependence of anisotropy of Earth's inner core. *Journal of Geophysical Research* 100: 9805–9816.

Song X and Helmberger DV (1998) Seismic evidence for an inner core transition zone. *Science* 282: 924.

Song X and Richards PG (1996) Seismological evidence for differential rotation of the Earth's inner core. *Nature* 382: 221–224.

Souriau A (1989) A search for time dependent phenomena inside the core from seismic data. In: *EGS Meeting Abstracts, Barcelona*.

Souriau A (1998) New seismological constraints on differential rotation of the inner core from Novaya Zemlya events recorded at DRV, Antarctica. *Geophysical Journal International* 134: F1–F5.

Souriau A (2009) Inner core structure: Constraints from frequency dependent seismic anisotropy. *Comptes Rendus Geoscience* 341: 439–445.

Souriau A, Garcia R, and Poupinet G (2003a) The seismological picture of the inner core: Structure and rotation. *Comptes Rendus Geoscience* 335: 51–63.

Souriau A and Poupinet G (1991) The velocity profile at the base of the liquid core from PKP(BC + C_{diff}) data: An argument in favor of radial inhomogeneity. *Geophysical Research Letters* 18: 2023–2026.

Souriau A and Poupinet G (2003) Inner core rotation: A critical appraisal. In: Dehant V, et al. (ed.) *Earth's Core, Dynamics, Structure and Rotation. Geophysical Monograph, Geodynamics Series*, vol. 31, pp. 65–82. Washington, DC: American Geophysical Union.

Souriau A and Romanowicz B (1996a) Anisotropy in inner core attenuation: A new type of data to constrain the nature of the solid core. *Geophysical Research Letters* 23: 1–4.

Souriau A and Romanowicz B (1996b) Anisotropy in the inner core: Relation between P-velocity and attenuation. *Physics of the Earth and Planetary Interiors* 101: 33–47.

Souriau A and Roudil P (1995) Attenuation in the uppermost inner core from broad-band GEOSCOPE PKP data. *Geophysical Journal International* 123: 572–587.

Souriau A, Roudil P, and Moynot B (1997) Inner core rotation: Facts and artefacts. *Geophysical Research Letters* 24: 2103–2106.

Souriau A and Souriau M (1989) Ellipticity and density at the inner core boundary from subcritical PKiKP and PcP data. *Geophysical Journal International* 98: 39–54.

Souriau A, Teste A, and Chevrot S (2003b) Is there any structure inside the liquid core? *Geophysical Research Letters* 30(11): 1567.

Stevenson DJ (1987) Limits on lateral density and velocity variations in the Earth's outer core. *Geophysical Journal of the Royal Astronomical Society* 88: 311–319.

Stroujkova A and Cormier VF (2004) Regional variations in the uppermost 100 km of the Earth's inner core. *Journal of Geophysical Research* 109: B10307.

Su WJ and Dziewonski AM (1995) Inner core anisotropy in three dimensions. *Journal of Geophysical Research* 100: 9831–9852.

Su W-J, Dziewonski AM, and Jeanloz R (1996) Planet within a planet: Rotation of the inner core of the Earth. *Science* 274: 1883–1887.

Suda N and Fukao Y (1990) Structure of the inner core inferred from observations of seismic core modes. *Geophysical Journal International* 103: 403–413.

Sumita I and Olson P (1999) A laboratory model for convection in Earth's core driven by a thermally heterogeneous mantle. *Science* 286: 1547–1549.

Sumita I, Yoshida S, Kumazawa M, and Hamano Y (1996) A model for sedimentary compaction of a viscous medium and its application to inner core growth. *Geophysical Journal International* 124: 502–524.

Sun X and Song X (2008) Tomographic inversion for the three-dimensional anisotropy of the Earth's inner core. *Physics of the Earth and Planetary Interiors* 167: 53–70.

Sze EKM and Van der Hilst RD (2003) Core mantle boundary topography from short period PcP, PKP and PKKP data. *Physics of the Earth and Planetary Interiors* 135: 27–46.

Tanaka S (2007) Possibility of a low P-wave velocity layer in the outermost core from global SmKS waveforms. *Earth and Planetary Science Letters* 259: 486–499.

Tanaka S (2012) Depth extent of hemispherical inner core from PKP(DF) and PKP (C_{diff}) for equatorial paths. *Physics of the Earth and Planetary Interiors* 210–211: 50–62.

Tanaka S and Hamaguchi H (1993) Degree one heterogeneity at the top of the earth's core, revealed by SmKS travel times. In: *Dynamics of Earth's Deep Interior and Earth's Rotation*. *IUGG/AGU Geophysical Monograph*, vol. 72, pp. 127–134. Washington, DC: IUGG/AGU.

Tanaka S and Hamaguchi H (1996) Frequency-dependent Q in the Earth's outer core from short period P4KP/PcP spectral ratio. *Journal of Physics of the Earth* 44: 745–759.

Tanaka S and Hamaguchi H (1997) Degree one heterogeneity and hemispherical variation of anisotropy in the inner core from PKP(BC)-PKP(DF) times. *Journal of Geophysical Research* 102: 2925–2938.

Tkalčić H and Kennett BLN (2008) Core structure and heterogeneity: Seismological perspective. *Australian Journal of Earth Sciences* 55: 419–431.

Tkalčić H, Kennett BLN, and Cormier VF (2009) On the inner–outer core density contrast from PKikP/PcP amplitude ratios and uncertainties caused by seismic noise. *Geophysical Journal International* 179: 425–443.

Tkalčić H, Romanowicz B, and Houy N (2002) Constraints on D″ structure using PKP (AB-DF), PKP(BC-DF) and PcP-P travel time data from broadband records. *Geophysical Journal International* 149: 599–616.

Tkalčić H, Young M, Bodin T, Ngo S, and Sambridge M (2013) The shuffling rotation of the Earth's inner core revealed by earthquake doublets. *Nature Geoscience* 6: 497–502.

Tromp J (1993) Support for anisotropy of the Earth's inner core from free oscillations. *Nature* 366: 678–681.

Tseng T-L, Huang B-S, and Chin B-H (2001) Depth-dependent attenuation in the uppermost inner core from the Taiwan short period seismic array PKP data. *Geophysical Research Letters* 29: 459–462.

Vidale JE, Dodge DA, and Earle PS (2000) Slow differential rotation of the Earth's inner core indicated by temporal changes in scattering. *Nature* 405: 445–448.

Vidale JE and Earle PS (2000) Fine-scale heterogeneity in the Earth's inner core. *Nature* 404: 273–275.

Vidale JE and Earle PS (2005) Evidence for inner-core rotation from possible changes with time in PKP coda. *Geophysical Research Letters* 32: L01309.

Vinnik L, Romanowicz B, and Bréger L (1994) Anisotropy in the center of the inner core. *Geophysical Research Letters* 21: 1671–1674.

Vočadlo L (2007) Ab initio calculations of the elasticity of iron and iron alloys at inner core conditions: Evidence for a partially molten inner core? *Earth and Planetary Science Letters* 254: 227–232.

Wahr J and de Vries D (1989) The possibility of lateral structure inside the core and its implications for nutations and Earth tide observations. *Geophysical Journal International* 99: 511–519.

Waszek L and Deuss A (2011) Distinct layering in the hemispherical seismic velocity structure of Earth's upper inner core. *Journal of Geophysical Research* 116: B12313, Correction (2012) *Journal of Geophysical Research* 117: B10304.

Waszek L, Irving J, and Deuss A (2011) Reconciling the hemispherical structure of Earth's inner core with its super-rotation. *Nature Geoscience* 4: 264–267.

Weber P and Machetel P (1992) Convection within the inner core and thermal implications. *Geophysical Research Letters* 19: 2107–2110.

Wen L (2006) Localized temporal change of the Earth's inner core boundary. *Science* 314: 967–970.

Wen L and Niu F (2002) Seismic velocity and attenuation structures in the top of the Earth's inner core. *Journal of Geophysical Research* 107(B11): 2273.

Wenk HR, Baumgardner JR, Lebensohn RA, and Tomé CN (2000) A convection model to explain anisotropy in the inner core. *Journal of Geophysical Research* 105: 5662–5677.

Widmer RG, Masters F, and Gilbert F (1991) Spherically symmetric attenuation within the Earth from normal mode data. *Geophysical Journal International* 104: 541–553.

Widmer RG, Masters F, and Gilbert F (1992) Observably split multiplets – Data analysis and interpretation in terms of large-scale aspherical structure. *Geophysical Journal International* 111: 559–576.

Wiechert E (1896) Uber die Beschaffenheit des Erdinneren. *Verhandlungen der Gesellschaft Deutscher Naturforscher und Ärzte* 2: 42.

Woodhouse JH, Giardini D, and Li X-D (1986) Evidence for inner core anisotropy from free oscillations. *Geophysical Research Letters* 13: 1549–1552.

Wookey J and Helffrich G (2008) Inner-core shear-wave anisotropy and texture from an observation of PKJKP. *Nature* 454: 873–877.

Yoshida S, Sumita I, and Kumazawa M (1996) Growth model of the inner core coupled with the outer core dynamics and the resulting elastic anisotropy. *Journal of Geophysical Research* 101: 28085–28103.

Yu W and Wen L (2006a) Seismic velocity and attenuation structures in the top 400 km of the earth's inner core along equatorial paths. *Journal of Geophysical Research* 11: B07308. http://dx.doi.org/10.1029/2005JB003995.

Yu W and Wen L (2006b) Inner core anisotropy in attenuation. *Earth and Planetary Science Letters* 245: 581–594.

Yu W and Wen L (2007) Complex seismic anisotropy in the top of the Earth's inner core beneath Africa. *Journal of Geophysical Research* 112: B08304.

Yu W, Wen L, and Niu F (2005) Seismic velocity structure in the Earth's outer core. *Journal of Geophysical Research* 110: B02302. http://dx.doi.org/10.1029/2003JB002928.

Yukutake T (1998) Implausibility of thermal convection in the Earth's solid inner core. *Physics of the Earth and Planetary Interiors* 108: 1–13.

Zhang J, Richards PG, and Schaff DP (2008) Wide-scale detection of earthquake waveform doublets and further evidence of inner core super-rotation. *Geophysical Journal International* 174: 993–1006.

Zhang J, Song X, Li Y, Richards PG, Sun X, and Waldhauser F (2005) Inner core differential motion confirmed by earthquake waveform doublets. *Science* 309: 1357–1360.

Zou Z, Koper K, and Cormier V (2008) The structure at the base of the outer core inferred from seismic waves diffracted around the inner core. *Journal of Geophysical Research* 113: B05314.